

Instrumentation of an Offshore Nautical Radar and platform with a sensor suite for measuring vibrations in situ

Christos Poirazis

July 2023

A thesis submitted to the Delft University of Technology in
partial fulfillment of the requirements for the degree of Master
of Science in Offshore & Dredging Engineering

Supervisors: Dr. A. Cicirello, TU Delft, Chair and supervisor
Dr. A. Cabboi, TU Delft
Dr. E. Lourens, TU Delft
Ir. S. van Aartsen, Rijkswaterstaat CIV



Rijkswaterstaat
Ministerie van Infrastructuur en Waterstaat

Christos Poirazis: *Instrumentation of an Offshore Nautical Radar and platform with a sensor suite for measuring vibrations in situ* (2023)



Abstract

Offshore nautical radar systems are exposed to harsh environmental conditions during their service life. The structure is subjected in return to multiple random vibrations. Assessing the impact that these vibrations have on the structural integrity of the radar is necessary for creating a concrete operation and maintenance plan, that can enable the avoidance of structural damage due to fatigue. The development of a sensor network for the long term monitoring of such vibrations can provide an insight into the structural behaviour of a structure and predict possible damage scenarios.

The objective of this thesis is to determine how to instrument an offshore nautical radar in order to monitor vibrations in operating conditions. To achieve such a feat, short term vibration measurements (for non-operating conditions) are performed on a 5.7-meter-long radar antenna that is supported by truss tower (or mast) with a height of 20 meters, located in Rijkswaterstaat's test site in Stellendam. The aim of this approach is initially to extract the modal properties of the two structures, examine their interaction, and gather relevant information that can facilitate the determination of what a future sensor network, for the long term monitoring of the antenna, could look like.

For the realization of such measurements two main system identification techniques are used along with a small sensor suite of accelerometers. Experimental Modal Analysis (EMA) is performed on the radar antenna, by approximating a laboratory setting with minimal environmental interference. The system's dynamic properties are extracted and analyzed critically in order to identify suitable sensor specifications and fitting sensor positioning among others. On the other hand, an Operational Modal Analysis (OMA) is executed on the truss tower in an attempt to see how its structural behaviour may affect the radar antenna's response and any future monitoring plan.

The results obtained from the aforementioned modal analyses, are employed to propose a long term sensor network for the radar antenna, along with monitoring techniques that can be used to achieve the goal of damage detection. What becomes also evident from the current approach, is the need of a better equipped sensor suite and a cross-validating Finite Element model, in order to achieve more robust results.

Acknowledgements

Throughout the period that took me to complete this thesis, there were a number of people that contributed to my academic and personal development.

First of all, I would like to thank my chair and daily supervisor, Dr. Alice Cicirello, who provided all the support, knowledge and tools required to complete this study. Her constant encouragement for further research and critical thinking was motivational and inspiring. I would also like to express my thanks to Dr. Alessandro Cabboi and Dr. Eliz-Mari Lourens, for their crucial advice and guidance whenever needed or requested by my side. I would also like to express my gratefulness to Simon van Aartsen for giving me the opportunity to be a part of this research project and for constantly contributing with his utmost enthusiasm and selfless assistance.

I would like to expand my gratitude to my fellow traveller on this journey, Vasileios Sfetsios, who throughout this period, managed to become a role model, a motivation and most importantly a dearest friend. Lastly, I would like to acknowledge the relentless support provided my family, which without it, I wouldn't even be in this privileged position.

...

Contents

1. Introduction	1
1.1. Motivation	1
1.2. Problem Statement	3
1.3. Research Objective	4
1.4. Approach	5
1.5. Thesis Outline	5
2. Experimental Modal Analysis	7
2.1. Assumptions and experimental set-up	7
2.2. Signal Processing	8
2.3. Frequency Response Function and modal parameters	10
2.4. Small-scale experiment and conclusions	11
3. Operational Modal Analysis	13
3.1. Assumptions and operational set-up	13
3.2. Natural Excitation Technique	13
3.3. Eigensystem Realization Algorithm	14
3.4. Numerical example and conclusions	17
4. Experimental Modal Analysis: Radar Antenna	19
4.1. Experiment Objective	19
4.2. Nautical radar components	19
4.3. Experiment design and Radar Instrumentation	19
4.4. Vibration Measurements	21
4.4.1. Metal Plate test	21
4.4.2. Radar antenna test	27
4.5. Conclusions	35
5. Operational Modal Analysis: Mast	37
5.1. Experiment objective	37
5.2. Structure description	37
5.3. Experiment design and mast Instrumentation	37
5.4. Methodology and Results	40
5.5. Conclusions	46
6. Future radar monitoring system proposal	49
6.1. Structural Health Monitoring and System Identification	49
6.2. Operational and environmental conditions	51
6.3. Sensor network proposal	53
6.3.1. Wireless Sensor Network	53
6.3.2. Sensor specifications	53
6.3.3. Sensor placement	54

Contents

7. Conclusions and Recommendations **57**
7.1. Conclusions 57
7.2. Recommendations 60

A. EMA daily log **61**

List of Figures

1.1. Brandaris lighthouse with the radar on top	1
1.2. Truss tower with the radar on top in the Offshore Expertise Center	2
1.3. Radar antenna and gear box on top of the mast	3
2.1. EMA excitation sources Cicirello [2020]	8
2.2. Typical shape of a Frequency Response Function	9
2.3. Half-power bandwidth method Cicirello [2020]	11
2.4. EMA on a suspended beam	12
2.5. Small-scale experiment Frequency Response Function	12
3.1. Comparison between real and identified *Eigensystem Realization Algorithm (ERA) Mode shapes	17
4.1. Radar on top of the mast	20
4.2. Radar dimensions in meters	20
4.3. Axis system	20
4.4. Metal plate	21
4.5. Metal plate bottom view schematic, point 12 as output point	22
4.6. Metal plate mount	23
4.7. Test set-up	23
4.8. Reciprocity check by exchanging hammer and accelerometer position between measurement points 1 and 2	24
4.9. Average Frequency Response Function: Measurement point 16	25
4.10. Average Frequency Response Function for all measurement points	26
4.11. Mode shape at 74 Hz	27
4.12. Mode shape at 174 Hz	27
4.13. Bottom part of radar antenna containing the metal plate points (11-20), along with the composite part ones (1-10, 21-30, 28 output point)	28
4.14. Different radar antenna views	29
4.15. Accelerometer mounted and secured with extra tape	29
4.16. Reciprocity check by exchanging hammer and accelerometer position between measurement points 2 and 9	30
4.17. Average Frequency Response Function: Measurement point 6	30
4.18. Average Frequency Response Function: Measurement point 11	31
4.19. Average Frequency Response Function for all measurement points	31
4.20. FRF amplitude close to Mode 1	32
4.21. FRF amplitude close to Mode 2	32
4.22. FRF amplitude close to Mode 3	33
4.23. FRF amplitude close to Mode 4	33
4.24. Mode Shape 2 at 23 Hz	34
4.25. Mode Shape 3 at 44 Hz	34
4.26. Mode Shape at 74 Hz	34

List of Figures

5.1. Different views of the mast	38
5.2. Mast elements	38
5.3. First two bending modes from Vasilis' finite element model Sfetsios [2022] . . .	39
5.4. Mast axis system along with the numbering and location of the its columns . .	39
5.5. Measurement points in column No. 1	40
5.6. Cross Spectral density of channel 2 and 3 (y-direction)	42
5.7. Impulse Response Functions for the y-direction (reference channel = 2)	42
5.8. Stabilization Diagram – y-direction	43
5.9. Cross Spectral density of channel 2 and 3 (x-direction)	44
5.10. Impulse Response Functions for the x-direction (reference channel = 2)	45
5.11. Stabilization Diagram – x-direction	46
6.1. A schematic of output-only parametric vibration-based damage detection meth- ods as described at Avci [2020]	51
6.2. Stress concentration from fatigue damage accumulation in FEM	55
6.3. Proposed sensor network configuration 1: 8 accelerometers and 6 strain gauges	55
6.4. Proposed sensor network configuration 1: 16 accelerometers and 6 strain gauges	56

List of Tables

4.1. Available measuring equipment	21
4.2. Selected parameters	22
4.3. Modal parameters for Mode 1	26
4.4. Modal parameters for Mode 2	26
4.5. Summary of the radar antenna's natural frequencies	35
5.1. First two natural frequencies of the mast	37
5.2. Measuring equipment for the mast vibrations tests	40
5.3. Welch's method parameters (y-direction)	41
5.4. Hankel matrix and truncation parameters (y-direction)	43
5.5. Identified modal properties for the y-direction	43
5.6. Welch's method parameters (x-direction)	44
5.7. Hankel matrix and truncation parameters (x-direction)	45
5.8. Identified modal properties for the x-direction	46
5.9. Comparison between natural frequencies from FEM and OMA	47
5.10. Summary of mast modes for both examined directions	47
7.1. Summary of the radar antenna's natural frequencies as presented in Chapter 4	58
7.2. Summary of mast modes for both examined directions as presented in Chapter 5	58
7.3. Identified parameters checklist	59

Acronyms

SI	System Identification	3
EMA	Experimental Modal Analysis	3
OMA	Operational Modal Analysis	4
FFT	Fast Fourier Transform	9
FRF	Frequency Response Function	7
FEM	Finite Element Method	11
DAQ	Data Acquisition System	9
ERA	Eigensystem Realization Algorithm	xi
NExT	Natural Excitation Technique	13
IRF	Impulse Response Function	41
MAC	Modal assurance criterion	42
SHM	Structural Health Monitoring	49
ML	Machine Learning	51
PSD	Power Spectral Density	50
WSN	Wireless Sensor Network	53

1. Introduction

1.1. Motivation

Rijkswaterstaat, the Ministry of Infrastructure and Water Management in the Netherlands, has been appointed to install offshore nautical radar systems for various purposes in the new North Sea wind farms. Current objective is for nautical radars to be installed on offshore wind farm substations, on top of specially designed masts and on top of specially designed platforms attached to the wind turbines. In order to ensure high durability (low maintenance costs) and effectiveness (high availability), the mechanical integrity of these systems needs to be assessed.

The purpose of this study is to determine how to instrument such an offshore nautical radar in order to monitor vibrations in operating conditions (i.e. while the radar antenna is rotating). The monitoring of vibrations can lead to important deductions about the radar's structural condition and facilitate the estimation of fatigue damage. The nautical radar's structural failure from fatigue damage is of special concern due to the failure of a similar radar on top of the Brandaris Lighthouse in the northern Netherlands. In 2015, the radar's rotating antenna, seen in [Figure 1.1](#), was torn, while loading conditions weren't regarded extreme enough to cause such a collapse. Vibration-based monitoring systems deal with the change in modal curvatures and natural frequencies, in order to identify damage accumulation [Das \[2015\]](#). So, the design of a robust long-term vibration monitoring system can prevent a similar failure by obtaining structural properties that can lead to conclusions about the structure's service life. This thesis defines appropriate instrumentation techniques and characteristics in order to achieve such a design.

In order Rijkswaterstaat to perform the task of long-term monitoring of the nautical radar and also avoid the complications of offshore conditions, a special test area was developed, the Offshore Expertise Centre in Stellendam. There, the radar of interest lies on top of a



(a) Radar before the incident



(b) Radar after the incident

Figure 1.1.: Brandaris lighthouse with the radar on top

1. Introduction



Figure 1.2.: Truss tower with the radar on top in the Offshore Expertise Center

mast (truss tower), as seen in [Figure 1.2](#) and [Figure 1.3](#). In order to be able to reach the goal of recommending a suitable measuring equipment for operating conditions, an experimental approach is being implemented, by developing techniques that aim to understand the physics of such a structure through modal analysis. These techniques involve short-term in-situ vibration measurements on the radar antenna and the mast for non-operating conditions. The aim of this strategy is firstly to determine a future sensor network that will enable damage detection that can facilitate the fatigue life estimation of the radar antenna. In addition, by performing vibration measurements on both the radar antenna and the mast, conclusions can be drawn on how the interaction between the two may affect the radar's response and in return its damage accumulation. Finally, the results of the current research can facilitate the update of the radar's Finite Element model that was developed as part of another TU Delft Thesis (by Vasilis Sfetsios [Sfetsios \[2022\]](#)).



Figure 1.3.: Radar antenna and gear box on top of the mast

1.2. Problem Statement

Modal testing constitutes a well established experimental method to identify a system's dynamic properties, meaning its natural frequencies, mode shapes and damping ratios. Vibration measurements frequently prove essential in modal analysis problems, being used either to refine analytical models or trouble-shoot complex vibration problems (Brandt [2011]).

The experimental analysis of vibrations is commonly performed by employing the use of sensors (e.g. accelerometers, strain gauges). Then, as part of the discipline of signal analysis, the sensor time signal is processed, usually in the frequency domain, providing useful results that help identify the properties of the dynamic system under examination.

Two main approaches exist when it comes to identifying a dynamic system from measurement data. Experimental Modal Analysis (EMA) is one way to determine the dynamic characteristics of a structure. It forms an input-output identification method, where a measured excitation force (input) and a measured response (output) are used to derive the so-called Frequency Response Functions (FRFs) that are the key to obtain the structure's modal parameters. Having both input and output data, EMA is considered a highly accurate System Identification (SI) technique. EMA is used frequently as the main system identification method in many small scale laboratory experiments (Pappalardo [2018], Bocca [2011], Tirelli [2011], Wu [2022]) but no cases of an EMA on a nautical radar have been found in literature. Experiments on larger scale field structures is also a common modal testing method (Venglar [2019], Cuhna [2006]), but usually large excitation devices are used, which are out of the scope of this thesis. That brings forth one main drawback of the EMA approach, which is that for large and complex structures, excitation from either a shaker or an instrumented hammer (the two main methods to apply a measured force on a system) doesn't necessarily provide enough energy to excite all relevant modes.

A way to counteract the above mentioned disadvantage is provided by the second main

1. Introduction

approach for System Identification, which is the Operational Modal Analysis (OMA). OMA forms an output-only identification method, where response data (output) come from ambient excitations, without measuring the applied force. The assumed force in this specific case would be wind, which behaves as band-limited white noise. The OMA approach is found extensively in the bibliography, either concerning the SI of bridges (Nayeri [2009], Cabboi [2016], Grimmelsman [2014]), wind turbines (Chauchan [2011]) or masonry towers (Gentile [2015]). With the use of specialized identification algorithms that use only output time-histories, the dynamic properties of a structure can be established. This fact is particularly interesting for performing measurements on a large scale structure like the mast.

In general, the instrumentation of the radar antenna poses many challenges. Although it is a beam-like structure, it is composed of many mechanical parts and its semi-hollow frame leaves a lot of questions to be answered regarding the correct positioning of sensors. The fact that no vibration analysis has been performed on a nominally identical radar complicates the problem at hand. Sensor specifications and sampling criteria can only be determined by recurring experimentation since structural behaviour is mostly unknown. This also means that the linear response of the structure, which is a main assumption for performing the SI methods investigated on this study, needs to be verified. In addition, specifically in the case of this study, material properties are not available.

In summary, by utilizing the above mentioned SI methods, and establishing several dynamic properties of the radar antenna and the mast, the main problem of instrumenting the radar under operating conditions, in order to detect and identify damages, will try to be solved.

1.3. Research Objective

The main objective of this research is to determine how to instrument a nautical radar system that is mounted on a mast structure, in order to monitor its vibrations on operating conditions. The necessary information for such a task is provided by performing a preliminary modal testing on the nautical radar and the mast while in non-operating conditions.

Based on the aforementioned objective, the main research question that arises is:

"How to instrument an offshore nautical radar mounted on a mast structure for monitoring vibrations in operating conditions?"

This question is accompanied with set of sub-questions that help identify the challenges of the research objective. These are:

- What kind of measurement equipment is suitable (e.g. accelerometer, DAQ) for monitoring vibrations on a rotating nautical radar?
 - Where should the sensors be placed on the radar?
 - How to determine expected amplitudes and frequency ranges by preliminary on-site measurements?

- How to distinguish the radar's dynamic response from the mast response?
 - How to monitor the vibration levels of the mast?
- How to collect and process the preliminary data for a non-rotating radar and a mast?
 - How to instrument preliminary the radar and the mast?
 - What signal processing methods are appropriate (e.g. sampling, filtering etc.)?
 - Which are the limitations of an output-only vs. an input-output system identification (SI) method for assessing the modal properties of the radar and mast?

1.4. Approach

In more detail, the research problem was approached by employing the two main SI methods mentioned in Section 1.2. Firstly, EMA was performed on a simple cantilever beam in laboratory conditions with a set of TU Delft measuring equipment. This step is crucial in order to gain familiarity with the measuring equipment that is also used subsequently for the modal tests performed on the radar and mast respectively. In addition, since the radar antenna resembles a beam-like structure, many of the dynamic properties and modal analysis processes are similar to the one of a simple beam. Then, EMA was performed on the radar antenna while on non-operating conditions (non-rotating radar) for the purpose of identifying the antenna's modal properties. What followed was the performance of OMA on the mast structure in order to identify its respective modal characteristics and assess its contribution to the radar antenna's vibrations. Lastly, the long-term monitoring implementation on the radar antenna on operating operating conditions is examined by employing the above results along with proven methods found on the literature.

1.5. Thesis Outline

By taking into account the above mentioned approach and the research objectives the outline of the thesis is presented as follows:

- Chapter 2 presents an overview of EMA principles, focusing on the approaches used for the current set of experiments
- Chapter 3 provides a look on the building blocks of OMA and the related algorithms that are employed for this thesis
- Chapter 4 focuses on the experimental campaign on the radar antenna and the identification of its modal properties
- Chapter 5 presents the OMA performed on the mast and discusses its interaction with the radar

1. Introduction

- [Chapter 6](#) reviews vibration-based damage detection methods and proposes an appropriate sensor network set-up for the long-term radar antenna monitoring
- [Chapter 7](#) summarizes the thesis outcomes and suggests future recommendations
- Appendix A presents a daily log of the measurement campaign on the radar antenna

2. Experimental Modal Analysis

Experimental Modal Analysis is a widely applied technique that enables the determination of the dynamic properties of the structure experimentally. It involves the excitation of the structure with a known force (input) and the measuring of the response (output). The structure under investigation is excited using different methods, such as impact hammers or shakers, while the response can be measured by sensors, such as accelerometers or strain gauges, that are attached at various locations on the structure. After the measurement data are acquired in the time domain, the signal is processed in order to extract the content in the frequency domain, usually by employing the Fast Fourier Transform (FFT). Then the modal parameters (natural frequencies, mode shapes and damping ratios) can be identified by using SI techniques, most commonly the Frequency Response Function (FRF), which is the method under investigation in the current research.

EMA is mostly appropriate for small and medium sized structures, as impact hammers and shakes can only produce a limited amount of energy, which in bigger structures may not be enough to excite all the modes of vibration of interest.

In this chapter, the building blocks of EMA are presented and analysed briefly in order to make evident how they can be applied on a structure like a radar antenna.

2.1. Assumptions and experimental set-up

Before examining how EMA works, the main assumptions need to be defined. First of all, the system under examination must behave linearly, meaning that the superposition principle must apply Brandt [2011]. The superposition principle says that, if an input $x_1(t)$ causes an output $y_1(t)$, and another input $x_2(t)$ causes an output $y_2(t)$, then for a linear system, the input signal $x_1(t) + x_2(t)$ will be $y_1(t) + y_2(t)$. Another assumption is that the structure is time invariant, and that the parameters that have to be determined are constant. In addition, Maxwell's reciprocity relation must be obeyed. The theorem shows that the frequency response between two points is the same if we excite in point q and measure the response in point p , as if we reverse the force and response points. Finally, the structure must be observable, meaning that a force applied at a point, as well the response that this force generates, should give away enough information to generate a representative model of the structure's behaviour.

As mentioned already in this chapter, the main excitation sources (input force) on EMA is either a shaker or a hammer (Figure 2.1). A shaker performs harmonic or random excitations while with the hammer impulse forces are achieved. Given certain advantages of the hammer over the shaker (portability, easy set-up, movable excitation point), it is selected as the most preferred excitation source and thus makes for the item of investigation during this study. An instrumented hammer features a force sensor that is integrated into the hammer's striking surface. The force sensor provides a measurement of the amplitude and the

2. Experimental Modal Analysis

frequency content of the energy stimulus that is caused on the test object. The input excitation frequency range is controlled mainly by the hardness of the tip selected. The harder the tip, the wider the frequency range that is excited by the excitation force.

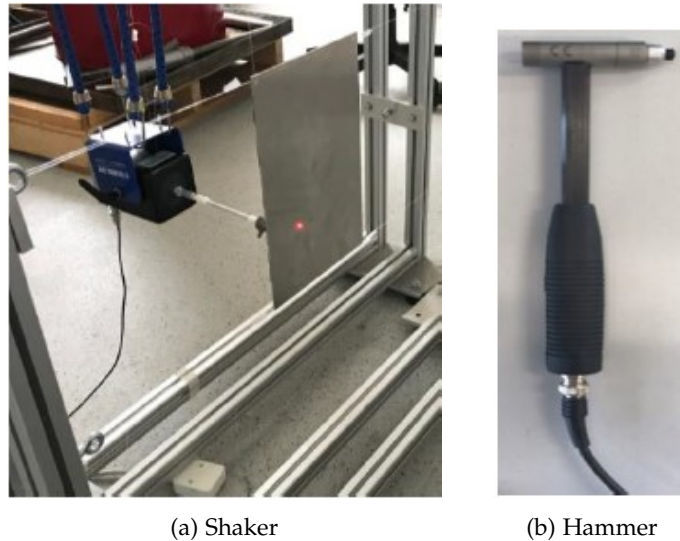


Figure 2.1.: EMA excitation sources [Cicirello \[2020\]](#)

In order to capture the structural vibration (response or output) of the structure, when excited from an input force, sensors are attached at specific locations. The sensors most suitable for *EMA* are either accelerometers or strain gauges. Strain gauges are out of the scope of this study, since they were not part of the available equipment. A piezo-electric accelerometer is a sensor that generates an electrical output proportional to the applied acceleration. It converts a physical parameter (acceleration) into an electrical signal, by employing the piezoelectric effect of certain materials. This voltage signal is later transmitted to a data acquisition system.

Two main methods exist regarding the placement of the sensors and the selection of impact points. The roving hammer technique involves exciting the structure at different locations using the impact hammer and measuring the response of one/multiple sensors distributed across the structure. On the other hand, *EMA* can be performed by keeping the excitation force on a specific position while the sensors are moved or re-positioned during the measurement process.

The measurements from the hammer and the sensors are recorded using the aforementioned data acquisition system, which capture the input's amplitude and frequency content and the time-domain response signals. The acquired data can be stored on a computer.

2.2. Signal Processing

Once the data mentioned in the previous section are assembled (amplitude and frequency content of the input and response signal from the output), the main aim of *EMA* in the frequency domain is to acquire the Frequency Response Function ([Figure 2.2](#)). *FRF* is the

relationship between the input applied at a point (impact force) i of a structure and the output (acceleration) measured at a point j of a structure. In more detail, is the complex ratio of the spectrum of the response r_j and force F_i respectively, each obtained by performing the Fast Fourier Transform (FFT) of the output and input time signals. Its mathematical expression can be seen on the Equation 2.4.

$$H_{ij}(\omega) = \frac{r_j(\omega)}{F_i(\omega)} \quad (2.1)$$

Where ω is the frequency

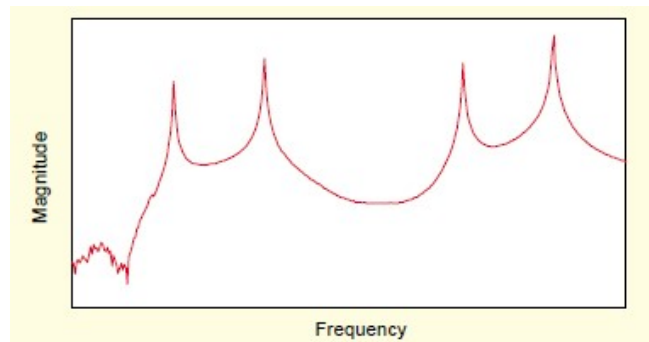


Figure 2.2.: Typical shape of a Frequency Response Function

In order though to be able to perform the FFT and in return acquire the FRF, the obtained signal needs to be processed accordingly, by applying specific signal filtering and windowing processes.

Firstly, the analog signal obtained from measurements must be filtered to ensure that there is no aliasing of the higher frequencies into the analysis frequency range. This is usually done by a low frequency pass anti-aliasing filter that must be applied before the analogue-to-digital conversion and thus is embedded in the Data Acquisition System (DAQ). In order to satisfy the Nyquist theorem, the signal must have no frequency content above half the sampling frequency.

After the digitization of the signal, a high-pass filter should be applied in order to remove the DC offset, occurring due to various factors such as imperfect circuitry, or external influences and forming an unwanted deviation from the expected zero level.

Following the filtering process is the windowing of the force and response signal. The force window is applied in order to ensure that the signal outside the range where there is a substantial force is down to zero. On the response signal, an exponential window is applied. If the response signal does not die out within the measurement time interval, then the periodicity requirement of the FFT is not met and the leakage effect comes into play when transforming data from time to frequency domain. So the exponential window assures that the free decay response becomes zero during the time interval, acting as artificial damping.

2.3. Frequency Response Function and modal parameters

After the application of the above signal processing techniques the amplitude of the FRF at each frequency can be obtained, by employing Equation 2.4 as indicated in the previous section. The general expression of the FRF in terms of acceleration (m/Ns^2) can also be expressed as:

$$H(w, x, y) = -\omega^2 \sum_n \frac{U_n(x)U_n(y)}{\omega_n^2 + i\omega\Delta_n - \omega^2} \quad (2.2)$$

where,

x is the driving point (input)

y is the observation point (output)

ω is the frequency

ω_n is the n_{th} natural frequency

$U_n(x)U_n(y)$ is the modal amplitude factor or a_n

Δ_n is the modal damping

Under the assumption that only one resonance is contributing to the response (low modal overlap) Equation 2.2 can be expressed as:

$$H(w, x, y) = -\omega^2 \frac{U_n(x)U_n(y)}{\omega_n^2 + i\omega\Delta_n - \omega^2} \quad (2.3)$$

While near resonance, where $\omega = \omega_n$, the above equation becomes:

$$H(w, x, y) = -\omega \frac{U_n(x)U_n(y)}{i\omega_n\Delta_n} = iQ_n a_n \quad (2.4)$$

where, Q_n is the Quality Factor, which shows how damped is the structure at a specific frequency, and is expressed as:

$$Q_n = \frac{\omega_n}{\Delta_n} \quad (2.5)$$

The estimation of Quality factor can be done by calculating the ratio between the natural frequency and the half-power bandwidth, i.e. the modal damping, which can be estimated by subtracting the lower and upper frequencies occurring from a 3dB drop from the FRF peak (Figure 2.3).

At this point, all the data needed to fully characterize a mode shape have been assembled. This can be achieved by estimating the modal amplitude factor a_n for each grid point. In the case that the roving hammer technique is employed, the grid points correspond to all the impact points. The selection of these points must be enough to capture the length and

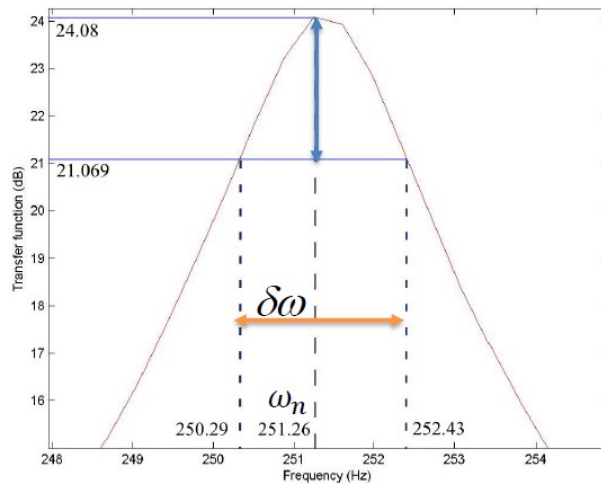


Figure 2.3.: Half-power bandwidth method [Cicirello \[2020\]](#)

width of a structure and in parallel they should not be a nodal point. A node is a point with no motion in the mode. To avoid that, multiple grid points must be chosen so the detection of the entire mode can be achieved, especially when there is no indication of nodal points from an already existing analytical or Finite Element Method (FEM) model.

2.4. Small-scale experiment and conclusions

In order to validate the theory and experimental process, and in parallel understand the signal processing mechanics, an experimental evaluation of the modal properties of a suspended aluminum beam was performed ([Figure 2.4](#)). The beam was suspended in such a way that a reproduction of free-free boundary conditions is achieved. An instrumented hammer was used to apply an impulsive force to the beam. A fixed position accelerometer was used to measure the response of 12 impact points distributed across the beam. A numerical model was used to avoid nodal points. MATLAB was used to process the signal and develop the modal properties of the beam.

The resulting FRF can be seen on [Figure 2.5](#). The extracted mode shapes were similar to the ones obtained from the numerical model, thus validating that all the EMA processes were applied correctly.

By taking into account the results of this small-scale experiment, it was proven that EMA can be used in a beam structure. As the radar antenna constitutes by itself a beam-like structure, the current methodology and equipment was deemed suitable to perform EMA in order to acquire its modal properties.

2. Experimental Modal Analysis

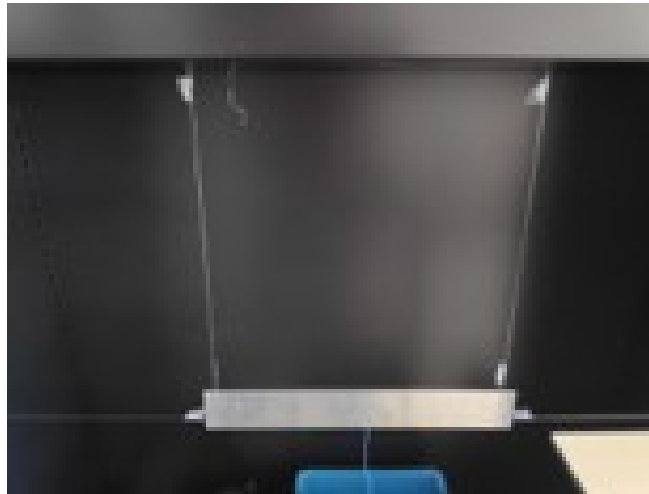


Figure 2.4.: EMA on a suspended beam

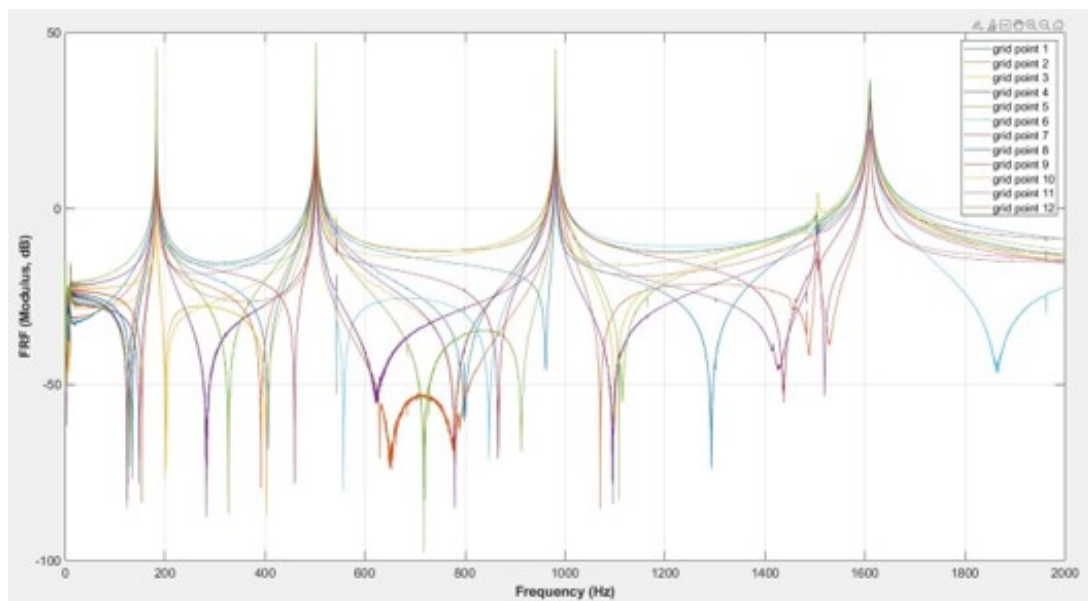


Figure 2.5.: Small-scale experiment Frequency Response Function

3. Operational Modal Analysis

Operational Modal Analysis constitutes an output-only methodology that does not require to measure the forces acting on the structure in order to identify a structure's modal properties (i.e the natural frequency, damping and mode shapes). In other words, it forms an identification technique that relies only on ambient vibrations in order to extract the modal parameters of a system.

Several OMA techniques are available in order to achieve modal identification. The current study employs the ERA along with the Natural Excitation Technique (NExT). ERA was developed by Juang and Pappa [1985] in order to be used for impulse excitation. NExT, which was developed by James [1995], can be used for records with the same characteristics that are utilized to create decaying response data from ambient vibration, enabling thus the use of the ERA.

According to Caicedo [2011], the NExT/ERA combination for modal identification has the following main steps. First, the vibration data are processed with NExT in order to be transformed into impulse responses. Then, by utilizing the ERA, the impulse functions are used to obtain the modal properties of the system. Finally the dynamic characteristics of the system are calculated.

3.1. Assumptions and operational set-up

Before analysing these OMA techniques, some key assumptions need to be made. First and foremost, the input loading should be considered a white noise stochastic process. If harmonic components are included in the input, then the algorithm may mistake harmonic modes as structural modes, resulting in a failure to correctly identify the system. A second assumption is that the structure behaves as a Linear Time-Invariant (LTI) system. This would mean that the relationship between input and output is linear and that during the time interval of the analysis the process remains stationary. Finally, the system states of interest need to be controllable (excited) and observable, similarly to EMA.

As mentioned already, OMA does not require measurement of the acting force and relies only on the response signal. This simplifies the set-up, meaning that only a number of sensors and a DAQ are required in order to extract sufficient data.

3.2. Natural Excitation Technique

The main idea behind NExT is that the cross-correlation function of the response will have the same properties as an impulse response, assuming that the input is a white noise stochastic process. The cross-correlation function $R_{xy}(t)$ between the outputs i and j , in the time domain, are expressed by Equation 3.1 (James [1995]).

3. Operational Modal Analysis

$$R_{ij}(t) = \sum_{l=1}^n \frac{\psi_{il} G_{j,l}}{m_l \omega_{d,i}} \exp(-\zeta_l \omega_{n,l} t) \sin(\omega_{d,l} t + \theta_l) \quad (3.1)$$

Where,

ψ_{il} is the i^{th} element of eigenmode l
 $G_{j,l}$ is a constant multiplier related to the input
 m_l is the l^{th} modal mass
 $\omega_{d,i}$ is the l^{th} damped natural frequency
 $\omega_{n,l}$ is the undamped natural frequency
 ζ_l is the modal damping ratio

In general, the cross-correlation function is a measure of similarity between 2 sets of data. The process involves the assessment of information between peak values. Practically, after the collection of the acceleration data, a reference channel is selected and then the cross-correlation function is estimated between the reference one and the other channels, in order to get the corresponding Instant Response Functions (IRFs). The reference channel serves as a baseline for comparison, helping to separate the modal responses from the effects of external excitations. It provides a well-characterized input signal that assists in the identification of modal frequencies, damping ratios, and mode shapes.

3.3. Eigensystem Realization Algorithm

In the description of ERA, it is stated that the algorithm works for impulse input. By using the impulse input obtained from NExT, an "OMA version" of ERA is introduced. Now, considering the state-space representation for a discrete system (Juang and Pappa [1985]):

$$\begin{cases} x_{k+1} = Ax_k + Bf_k \\ y_k = Cx_k + Df_k \end{cases} \quad (3.2)$$

Where,

x is the vector of states
 u is the vector of inputs
 y is the vector of outputs
 k is the time step ($t_k = k\Delta t$)
and A , B , C , and D are the discrete-time state-space matrices

In general, the eigensystem realization algorithm uses the principles of minimum realization to obtain a state-space representation of a system. The term realization means an estimation of the state-space matrices from the response of system. The eigenvalues of A are complex conjugates that correspond to a mode of vibration. Based on the matrices A and C , the

modal properties of the system can be estimated (B and D cannot be used in combination with NExT as the inputs of the system are unknown).

First step is to form the Hankel matrix (Equation 3.3), where p and q are the number of columns and rows of the Hankel matrix and Y_k is one block in the Hankel matrix, with rows equal to the number of output channels.

$$H_{k-1} = \begin{bmatrix} Y_k & Y_{k+1} & \dots & Y_{k+q-1} \\ Y_{k+1} & Y_{k+2} & \dots & Y_{k+q} \\ \dots & \dots & \dots & \dots \\ Y_{k+p-1} & Y_{k+p} & \dots & Y_{k+p+q-2} \end{bmatrix} \quad (3.3)$$

What follows is the singular value decomposition of H_0 (Equation 3.4). H_0 is the block Hankel matrix for $k=1$, and along with H_1 are used to obtain a realization of the system. U and V are orthogonal, and S is the matrix which includes the singular values of H_0 . The first diagonal non-zero values of S represent the order of the system.

$$H_0 = USV^T = (US^{1/2})(S^{1/2}V^T) \quad (3.4)$$

Under ideal conditions, only the first diagonal values of the S matrix would be non-zero and the true order of the system would be apparent. But since there is noise in real data, all the diagonal values of the S matrix are non-zero. That means that a truncation of the matrix should take place in order to find the true order of the system. Since there is no practical way to define that, multiple iterations are performed with different number of system order every time (different matrix truncation), until stable modes are identified. This forms the basis for the stabilization diagram. The truncated version of H_0 is presented in Equation 3.5

$$H_0 \approx U_n S_n V_n^T = (U_n S_n^{1/2})(S_n^{1/2} V_n^T) \quad (3.5)$$

After the minimum realization of the system has been obtained (i.e. the matrix truncation is completed), the system matrix A can be obtained as shown in Equation 3.6.

$$\begin{aligned} H_1 &= U_n S^{1/2} A S^{1/2} V_n^T \rightarrow \\ A &= S^{-1/2} U_n^T H_1 V_n S^{-1/2} \end{aligned} \quad (3.6)$$

By solving the eigenvalue problem of A (which includes all the dynamic properties) the eigenvalues Λ_d and eigenvectors Ψ_d can be derived.

$$\begin{aligned} \Lambda_d &= \text{diag}(\lambda_1, \lambda_2, \dots, \lambda_n) \\ \Psi_d &= [\psi_1, \psi_2, \dots, \psi_n] \end{aligned} \quad (3.7)$$

After deriving the eigenvalues, they will be converted from discrete-time to continuous time domain using Equation 3.8

3. Operational Modal Analysis

$$\begin{aligned}\Lambda &= \ln(\Lambda_d) / \Delta t \\ \Psi &= \Psi_d\end{aligned}\tag{3.8}$$

The natural frequency and the damping ratios of the system are obtained from the real and the imaginary part of each obtained complex pair of eigenvalues as shown in [Equation 3.9](#) and [Equation 3.10](#).

$$\omega_{d,i} = \text{Im}(\lambda_i)\tag{3.9}$$

$$\zeta_i = -\frac{\text{Re}(\lambda_i)}{|\lambda_i|}\tag{3.10}$$

Finally the mode shapes can be estimated from the multiplication of matrix C with the eigenvectors ([Equation 3.11](#)).

$$\Phi = C\Psi\tag{3.11}$$

The correlation between the identified mode shapes at a specific frequency can be compared using the MAC. The MAC value is a metric used to determine the similarity (linearity) of one-mode shape when compared with another reference mode. The MAC value ranges between 0 and 1, where a value of 1 indicates perfect similarity or correlation between two mode shapes, and a value of 0 indicates no similarity or correlation. MAC is calculated based on the orthogonality property of mode shapes. By using this criterion, one can filter the stabilization diagram, as modes with a MAC factor below a certain level are considered computational or noise modes.

$$MAC = \frac{|\tilde{q}_i^* q_i^*|}{\sqrt{|\tilde{q}_i^* q_i^*| |q_i q_i^*|}}\tag{3.12}$$

One main challenge is to specify the number of columns and rows of the Hankel matrix. This is further confirmed by the fact that different literature papers suggest different rules of thumb. [Nayeri \[2009\]](#) mentions that the number of columns should cover the most significant part of the cross-correlation time history, while he suggests the number of rows to be more than 20 times the number of expected modes. On the other hand [Caicedo \[2011\]](#) suggests the number of columns to be four times the number of expected modes. What was followed eventually as a guideline in the course of this research, was the practical suggestions from [Gasparis \[2019\]](#), which suggest the number of columns to cover the decaying section of the correlation function and the number of rows to be determined by iterative procedures.

3.4. Numerical example and conclusions

In order to validate the theory explained on the previous section, a simple example of identification of a 2-DOF system was performed on Matlab. A two-story building was represented as a coupled system with two point masses, with known dynamic properties (mass, stiffness, eigenvalues). The system was subjected to an impulse excitation with added uncertainty (generated on Matlab) in order to simulate Gaussian white noise, and then the modal properties were calculated by employing the Eigensystem Realization Algorithm (based on algorithm developed by Al-Rumaithi [2022]). Figure 3.1 shows how the modes obtained from the algorithm are compared with the real modes of vibration, revealing the close similarity between them.

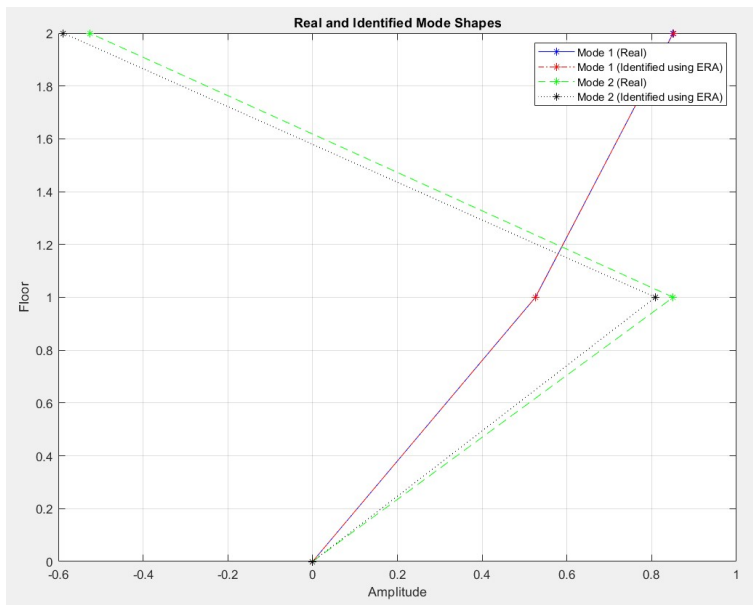


Figure 3.1.: Comparison between real and identified *ERA Mode shapes

By taking into account this small validation, it becomes apparent that when ERA is fed with impulse-like input, the modal parameters of a system can be extracted quite accurately. The combination of this method along with NEXT, which can translate ambient data to impulse-like data, makes for an appropriate OMA technique, that can facilitate the identification of the modal properties of the mast or any other structure under ambient excitation. As it will become apparent in Chapter 5, modal identification can be largely limited by the number of observable points and in return Degrees of Freedom, but nonetheless, even with a limited sensor network, results can be obtained, making OMA a powerful tool for identifying a system's dynamic characteristics.

4. Experimental Modal Analysis: Radar Antenna

4.1. Experiment Objective

As already discussed in [Chapter 1](#) and shown in [Chapter 2](#), EMA comprises the most fitting method in order to identify the radar antenna's dynamic properties. It forms a more deterministic approach than [OMA](#) and the structure's size allows the excitation energy to be transmitted all across the radar antenna's length. Measurements on the radar antenna took place on the Offshore Expertise Center in Stellendam. The main motivation behind this set of experimental measurements is initially to identify the natural frequencies, damping ratios and mode shapes of the radar antenna and in return define characteristics like frequency and acceleration ranges, modal nodes and sampling ratios that will facilitate the proposal of an appropriate sensor network for the long-term monitoring. Important to mention at this point is that the materials that comprise the radar antenna were unknown, thus the research was performed without taking into account any material properties.

4.2. Nautical radar components

The nautical radar system consists of two main components, the rotating radar antenna and its gearbox. It is supported by a pedestal, which is fixed on the truss tower, as seen in [Figure 4.1](#).

In more detail, the rotating antenna comprises a composite part and from a supporting metal (assumed) plate in the bottom, that is bolted on it. The antenna is connected with the gearbox through a rotating joint, that rotates along with the antenna. An illustration with all the relevant dimensions in meters is demonstrated in [Figure 4.2](#).

4.3. Experiment design and Radar Instrumentation

An axis system for the radar antenna was chosen as seen in [Figure 4.3](#). Since the two main forces that result from wind flow is the drag force (along the y-direction) and lift force (along the z-direction), the vibration measurements are focused on these two principal directions. In addition, in order to distinguish the the local modes of the plate from the global modes that concern the whole antenna, a separate measurement test was considered only for the metal plate, resulting in three separate set of tests, as listed below:

- Metal plate test (z-direction)

4. Experimental Modal Analysis: Radar Antenna



Figure 4.1.: Radar on top of the mast

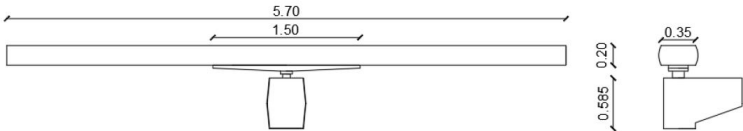


Figure 4.2.: Radar dimensions in meters

- Radar antenna test (z-direction)
- Radar antenna test (y-direction)

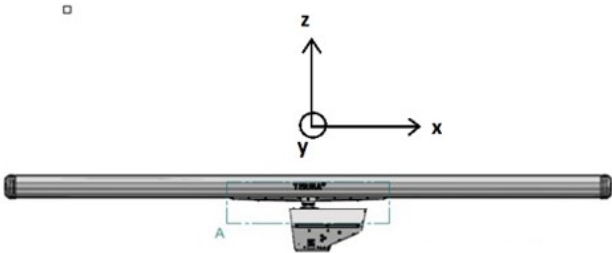


Figure 4.3.: Axis system

The available measuring equipment comprised a set of 4 accelerometers, an impact hammer and a Data Acquisition System (DAQ). The hardware’s specifications are visible in [Table 4.1](#). The hammer also was accompanied by different materials, that excite different ranges of frequencies. The software for recording the acceleration signals was the commercial software SignalExpress, while signal processing and system identification was performed on

Matlab.

Table 4.1.: Available measuring equipment

Equipment	Measurement range	Sensitivity	Frequency range	Axis type
PCB_352a21	500 g pk	10 mV/g	1-10000 Hz	uniaxial
PCB_352a24	50 g pk	100 mV/g	1-10000 Hz	uniaxial
PCB_356a44	100 g pk	50 mV/g	0,7-7000 Hz	triaxial
PCB_356a45	50 g pk	100 mV/g	0,7-7000 Hz	triaxial
ICP Impact Hammer	500 lbf pk	10 mV/lbf	-	-
DAQ-NI USB-443x	-	-	-	-

4.4. Vibration Measurements

4.4.1. Metal Plate test

Vibration measurements initially took place on the metal plate that supports the radar antenna and forms the contact point with the rotating joint. From Figure 4.4 is visible how the metal plate interfaces with the rest of the antenna.

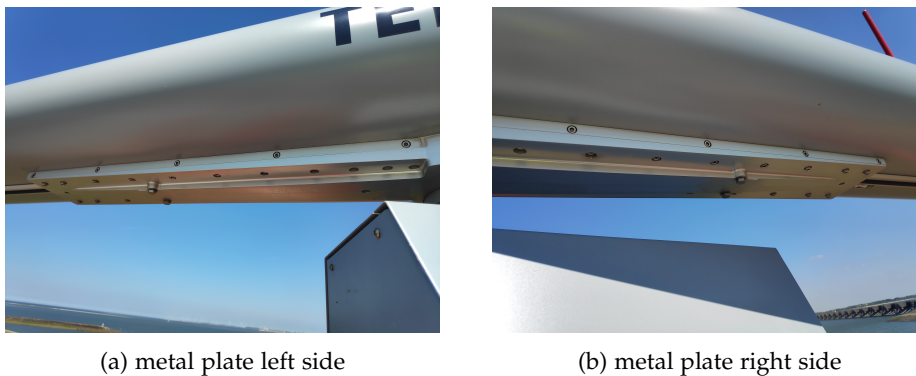


Figure 4.4.: Metal plate

Ten impact points (hereinafter called measurement points) were distributed across the metal plate length in order to measure the vibrations in the z-direction, which are visible in the schematic in Figure 4.5 (Points 11-20, Numbering follows the numbering scheme for the whole antenna). In order to evaluate the yet unknown acceleration amplitudes and frequency ranges of the plate, different sampling frequencies, accelerometers and impact hammer tips were tried. Eventually, the chosen sensor sensitivity ensured a good dynamic range (signal clipping avoidance), while the sampling frequency was set 10 times higher than the highest excited frequency in the force spectrum. The metal tip was used due to the fact that with softer tips the double tapping effect could not be avoided. The metal tip also excites the widest frequency range, making appropriate for the test. In the end, accelerometer PCB_352a24 was selected. Table 4.2 presents an overview of the test parameters. In Appendix A the whole selection process is analyzed and described.

4. Experimental Modal Analysis: Radar Antenna

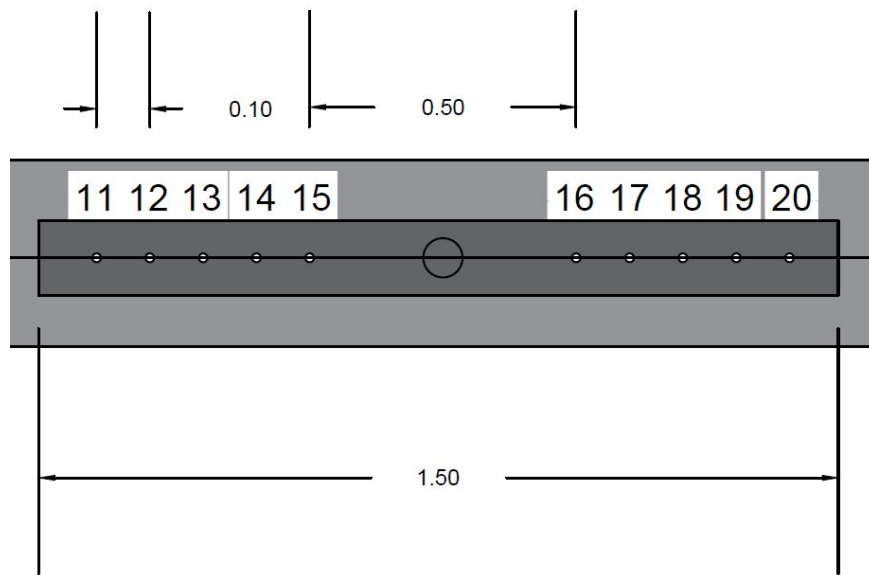


Figure 4.5.: Metal plate bottom view schematic, point 12 as output point

Table 4.2.: Selected parameters

Sampling frequency	20 kHz
Measurement range	50 g pk
Sensitivity	100 mV/g
Hammer tip	Metal

During every experiment session, the accelerometer was mounted on the plate with a quick bonding gel (Loctite 454), and its cable was secured with tape on the pedestal, as seen in [Figure 4.6](#). A check that is firmly mounted was always performed and its removal was done with the help of acetone. Point 12 was chosen as the output measurement point because it is closer to the edge of the plate, where bigger amplitudes were expected. The roving hammer method was used by applying 5 impacts per measurement point, along with a driving point measurement that was performed really close to the accelerometer. A reciprocity test was also executed. As it can be detected by a closer look at [Figure 4.4](#), the gearbox was impeding impacts with the hammer closer to the joint, and that's why there is a 50cm gap between measurement points 15 and 16. The experiment was performed over the course of two days, with the temperatures level being between 1 °C, and 3 °C, while the wind was at the level of 1-2 Beaufort. [Figure 4.7](#) shows the test set-up at the top of the mast. An extensive daily log, containing all the test details is featured in [Appendix A](#).

Results

The approach taken in this project is to extract sufficient data to properly identify the dynamic properties of the radar antenna and use them to propose a well fitting sensor network



Figure 4.6.: Metal plate mount

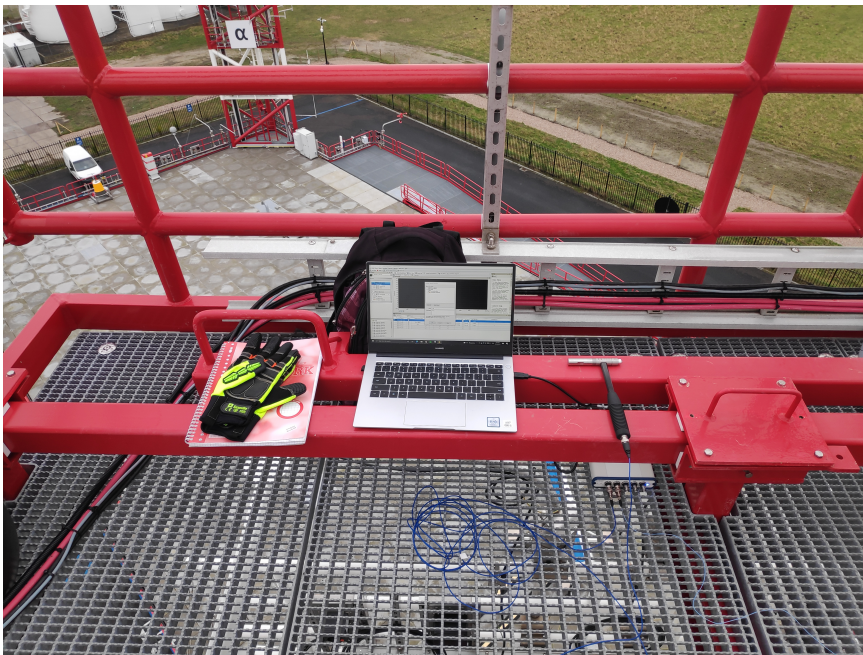


Figure 4.7.: Test set-up

4. Experimental Modal Analysis: Radar Antenna

for long-term monitoring. By taking this into account, along with the EMA theory values presented in Chapter 2 the following data processing procedure was followed:

- Anti-aliasing filtering to satisfy Nyquist theorem
- Windowing of the force and acceleration signals to remove noise and satisfy FFT periodicity respectively
- Reciprocity check (ensure linear structure response)
- Extraction of the average FRF for each measurement point
- Estimation of the natural frequencies and damping ratios
- Extraction of mode shapes

As mentioned previously, sampling frequency was set at 20 kHz, which was much more than the needed one to satisfy the Nyquist theorem. As you will notice later in this chapter, all of the clear modes occur within the first 200 Hz. After applying a rectangular window on the force signal and an exponential window on the acceleration signal, a reciprocity investigation was performed in order to check if the Maxwell's reciprocity relation stands. It is evident from Figure 4.8 that the response between the two points is quite similar.

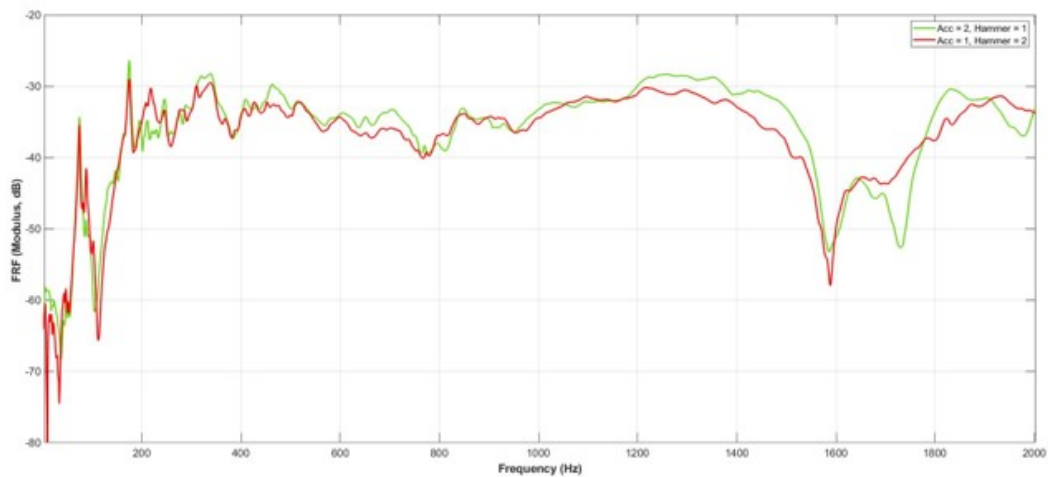


Figure 4.8.: Reciprocity check by exchanging hammer and accelerometer position between measurement points 1 and 2

After averaging the FRF for each one of the measurements points, it became apparent from the coherence factor that the noise within the first 40 Hz was significant. This could be attributed to numerous reasons. First of all, measurements took place in a real conditions, thus the lower frequencies of environmental loading (i.e. the wind) not only contributed directly to the vibrations of the radar but also indirectly due to the vibrations of the mast. In addition, wind may have caused movement of the accelerometer cable close to the connection of the two, thus introducing extra low frequency vibrations unrelated to the hammer input. At last, DC offset is also contributing to noise below the level of 5 Hz. After this frequency

threshold, coherence only appeared in anti-resonances, thus making the measurements results trustworthy. Figure 4.9 presents the FRF of point 16 up until the 400 Hz frequency, while its coherence function is representative of the FRFs of the rest of the measurements points.

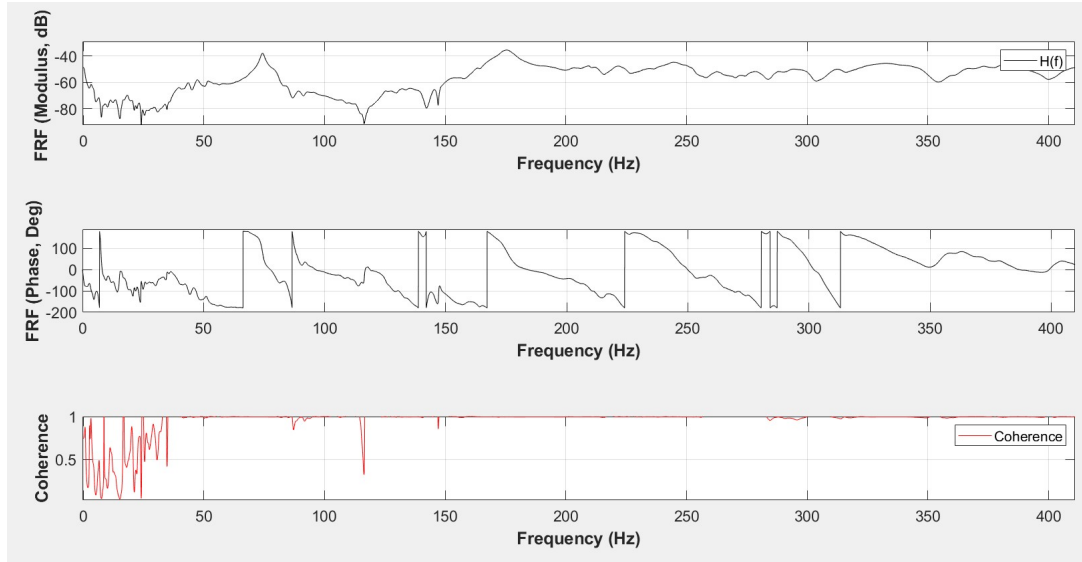


Figure 4.9.: Average Frequency Response Function: Measurement point 16

The FRFs for all the metal plate measurement points up until the 400 Hz mark are visible in Figure 4.10 (Point 1 is missing as impacting there was unachievable without signal clipping). There are two clear modes shapping within this frequency range, one at 74 Hz and the other at 174 Hz, while after the 200 Hz mark structure coupling impedes any further mode identification. For each one of the FRFs and modes, a Quality factor was calculated by employing the Half-power bandwidth method for damping. Nyquist plots were also employed to check whether the imaginary vs real part of the peak of the FRFs were forming a circle.

After calculating the scaled modal amplitudes at the measurement points, the apparent mode shapes for the two natural frequencies were estimated. Table 4.3 and Table 4.4 present the estimated modal parameters for each one of the modes. One can notice that there is a clustering effect on the quality factors among the the modes. Quality factors 2 through 5 and 6 through 10 present a difference in average values (e.g On mode 1, $Q_{avg}(12-15) = 27$, while $Q_{avg}(16-20) = 41$). This is attributed to the fact that the joint absorbs some of the excited energy resulting on different damping ratios for the the two areas left and right of the joint.

The two resulting mode shapes, after scaling the amplitudes from -100 to 100 are shown in Figure 4.11 and Figure 4.12. The first mode shape, at 74 Hz, seems to have some irregularities in its symmetry and also looks similar to mode shape 2. As it will be seen later on this chapter, the natural frequency of 74 Hz is also one of the natural frequencies of the whole radar antenna and its mode shape in the metal plate area looks very similar to a part of the radar antenna mode shape. So the fact that this local mode shape is part of a global mode shape, could justify both the irregularities in its symmetry (in larger scale the irregularities become minimal) and the resemblance with mode 2 (it is just a part of the global mode that

4. Experimental Modal Analysis: Radar Antenna

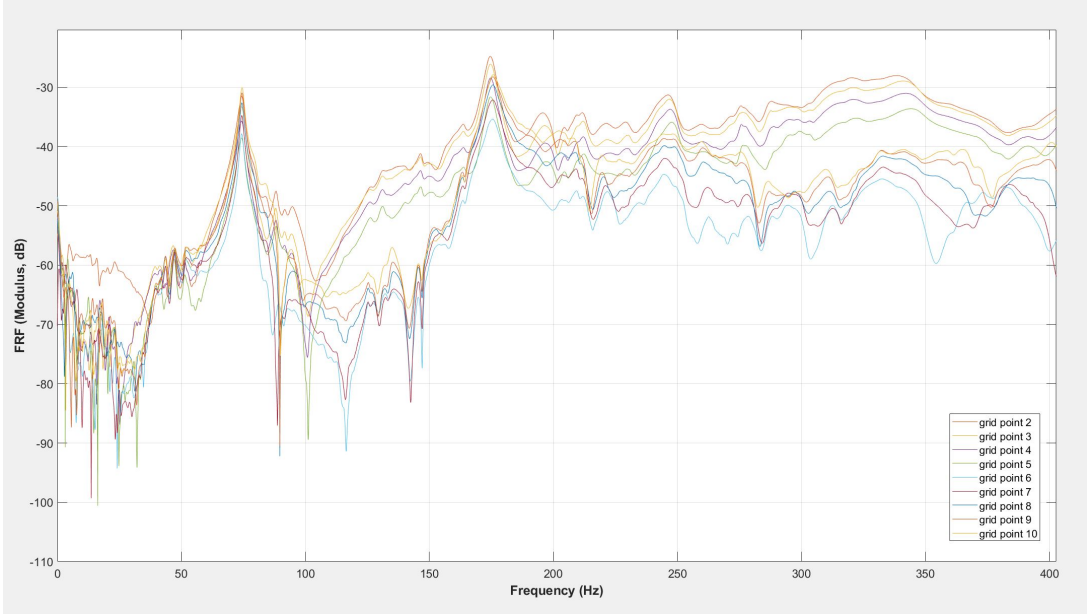


Figure 4.10.: Average Frequency Response Function for all measurement points

Table 4.3.: Modal parameters for Mode 1

Measurement points	Natural Frequency	Quality Factor	Modal amplitude factor
12	74.36	27.51	-0.00087
13	74.30	27.93	-0.00077
14	74.30	27.52	-0.00059
15	74.26	26.91	-0.00043
16	74.34	41.76	0.000305
17	74.36	42.25	0.000428
18	74.42	40.89	0.000566
19	74.44	40.02	0.0007
20	74.48	39.20	0.000786

Table 4.4.: Modal parameters for Mode 2

Measurement point	Natural Frequency	Quality factor	Modal amplitude factor
12	174.56	33.70	-0.00139
13	174.66	33.85	-0.00119
14	174.68	33.85	-0.00092
15	174.76	33.87	-0.00064
16	175.44	25.06	0.000563
17	175.54	25.81	0.000793
18	175.64	25.60	0.001069
19	175.68	24.88	0.001288
20	175.86	23.89	0.001397

resembles the local mode shape 2). Mode shape 2 on the other hand is anti-symmetric and its natural frequency unique to the metal plate (mode not identified on the whole antenna measurements).

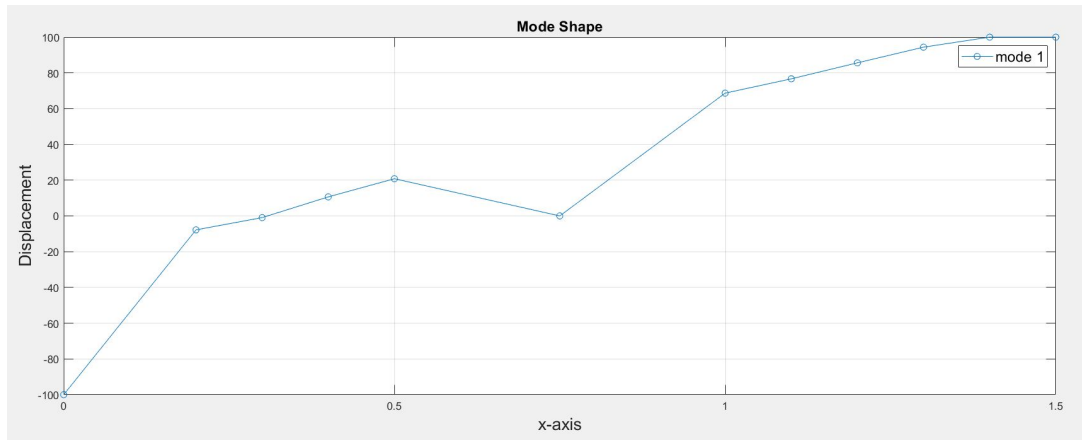


Figure 4.11.: Mode shape at 74 Hz

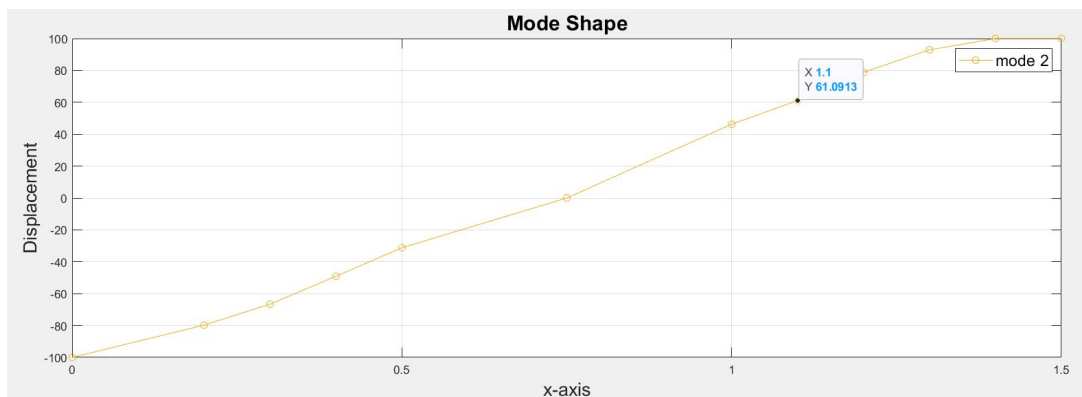


Figure 4.12.: Mode shape at 174 Hz

4.4.2. Radar antenna test

As mentioned previously, the radar antenna vibration tests included both the metal plate and the composite part of the material. Experiments were originally planned for both the z and y directions, according to the suggested axis system (Figure 4.3), but the measurements in y direction were abandoned. The reason was that the antenna composite part was interfacing with only a styrofoam-like material from the inside on its two longitudinal sides (Figure 4.14a), thus not allowing any vibrations to be transmitted across its length. For the z-direction, 30 impact points were distributed across the length of the antenna's bottom part (Figure 4.14b), 10 of them on the metal plate (the ones used for the previous experiments) and another 20 on the two respective sides of the antenna. The bottom part of the antenna was only considered, since the upper part was too high to perform any measurements. The last

4. Experimental Modal Analysis: Radar Antenna

60 cm from the antenna's respective edges were outside the platform's limits, making them unreachable for vibration testing. The schematic on [Figure 4.13](#) includes all the measurement point details, while [Figure 4.14](#)

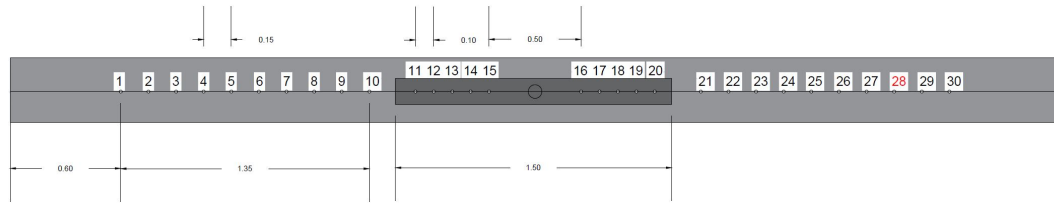


Figure 4.13.: Bottom part of radar antenna containing the metal plate points (11-20), along with the composite part ones (1-10, 21-30, 28 output point)

The same procedure as with the metal plate was followed in order to define the suitable sensor equipment and define the necessary parameters. Eventually, **PCB_352a24** was again selected as the output channel, while the test parameters were the same as in the metal plate test ([Table 4.2](#)). The same stands for the mounting procedures, with the difference that this time the cable was also secured by tape close to the accelerometer to avoid the low frequency noise that was noticed during the metal plate experiments ([Figure 4.15](#)). Point 28 was chosen as the output measurement point, because it is closer to the edge of the antenna, where bigger amplitudes were expected. The roving hammer method was again used by applying 5 impacts per measurement point, along with a driving point measurement that was performed really close to the accelerometer. A reciprocity test was executed anew. The experiment was performed over the course of four days with the temperatures level being between 5 °C, and 10 °C, while the wind was at the level of 2 Beaufort. As with the metal plate tests, an extensive daily log, containing all the test details is featured in [Appendix A](#).

Results

The signal processing methods that were employed for the metal plate were also used for the radar antenna case. Maxwell's reciprocity relation was again validated, as shown in [Figure 4.16](#)

For these sets of test, coherence factor showed again noisy data in the lower frequencies. One noticeable difference with the metal plate test is that the coherence factor in the composite material region is good way before the 40 Hz mark (coherence is generally equal to 1 after the 10 Hz mark), while in the metal plate region the coherence results resemble the ones from before (coherence is equal to 1 after the 40 Hz mark). Though the conclusions about the cause of noise in the lower frequencies remain mostly the same, it is uncertain if securing the cable with the extra tape contributed, since the noise region for the plate part is unchanged ([Figure 4.17](#) and [Figure 4.18](#)).

The FRFs for all the measurement points up until the 200 Hz mark are visible in [Figure 4.19](#), along with an indication to which peak corresponds to what mode (Driving point measurement data (28) was unachievable because of signal clipping). There are 4 clear modes shaping within this frequency range, one at 4,5 Hz, one at 23 Hz, one at 44 Hz and one in 74

4.4. Vibration Measurements



(a) antenna side view (y-direction)



(b) antenna bottom view (z-direction)

Figure 4.14.: Different radar antenna views



Figure 4.15.: Accelerometer mounted and secured with extra tape

4. Experimental Modal Analysis: Radar Antenna

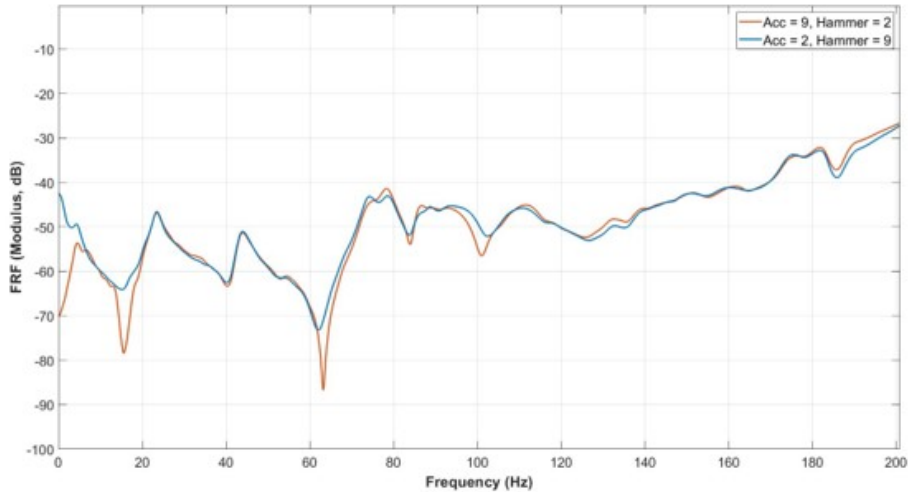


Figure 4.16.: Reciprocity check by exchanging hammer and accelerometer position between measurement points 2 and 9

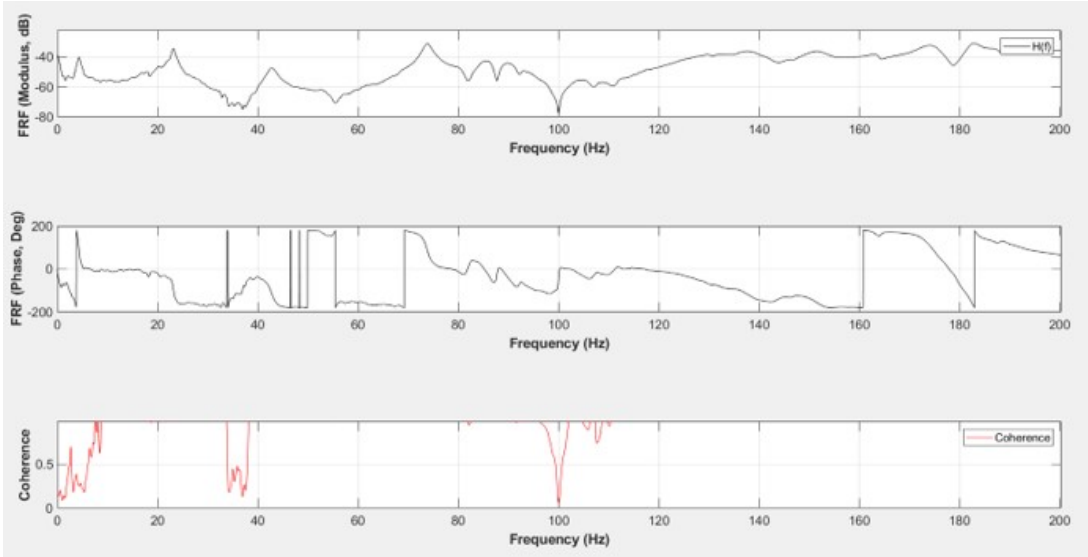


Figure 4.17.: Average Frequency Response Function: Measurement point 6

Hz while after the 80 Hz mark structure coupling impedes any further mode identification. By taking a closer look at the first, it can be observed that the FRFs of the plate’s measurements points (marked) present really high damping values. This fact along with the low coherence at this frequency level eventually couldn’t lead to a clear mode shape, though a natural frequency is clearly observable (Figure 4.20). Clustering of Quality Factors reappears also for the remaining 3 modes, this time also between the metal plate and the composite part. Metal plate modes present higher damping values that is most possibly caused by the different material of the two different radar components (Figure 4.21-Figure 4.23).

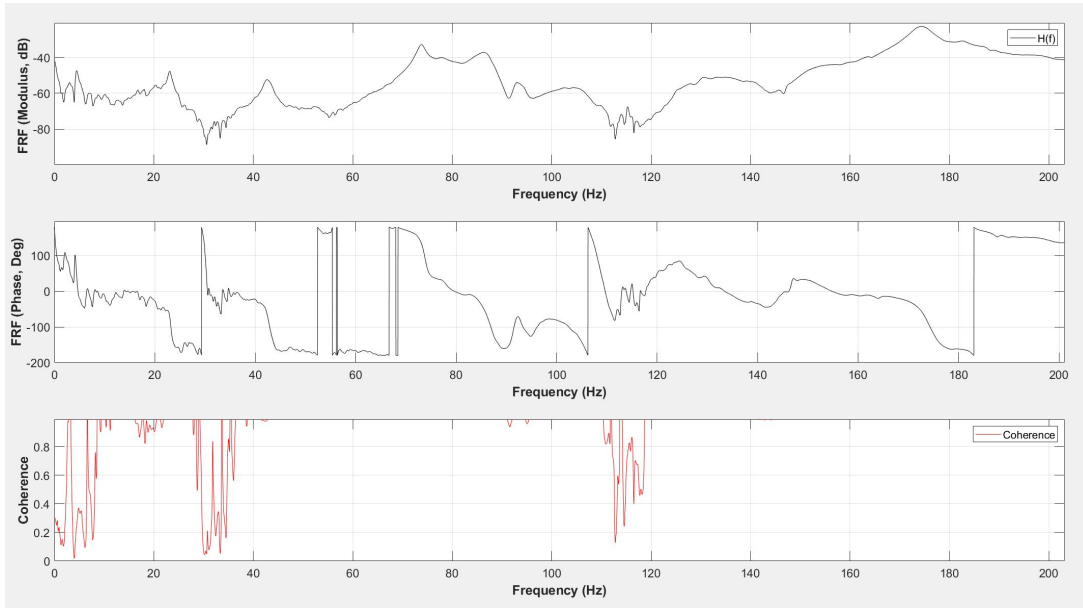


Figure 4.18.: Average Frequency Response Function: Measurement point 11

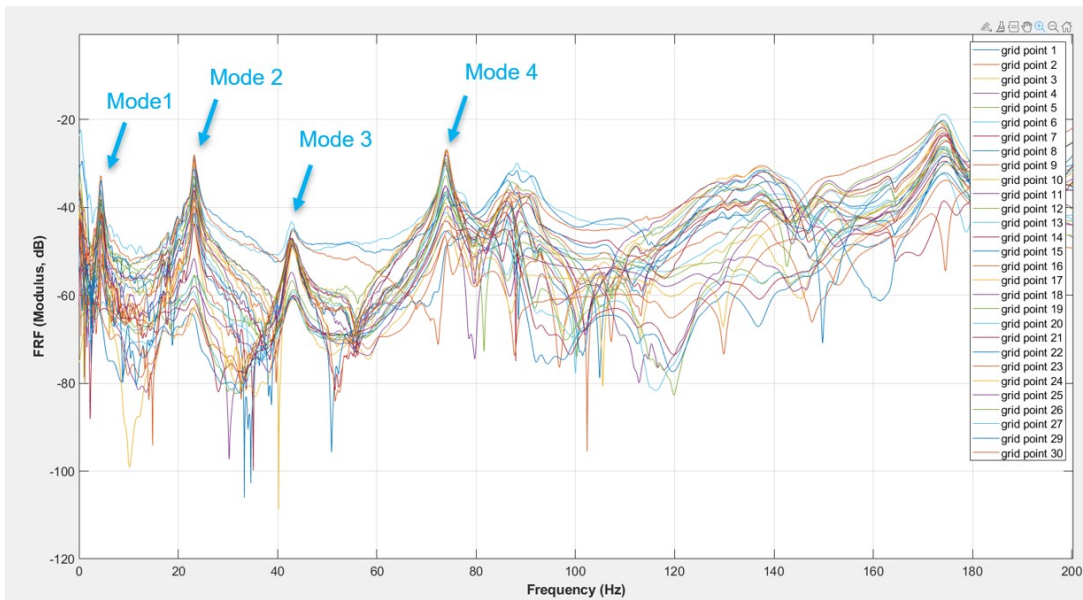


Figure 4.19.: Average Frequency Response Function for all measurement points

4. Experimental Modal Analysis: Radar Antenna

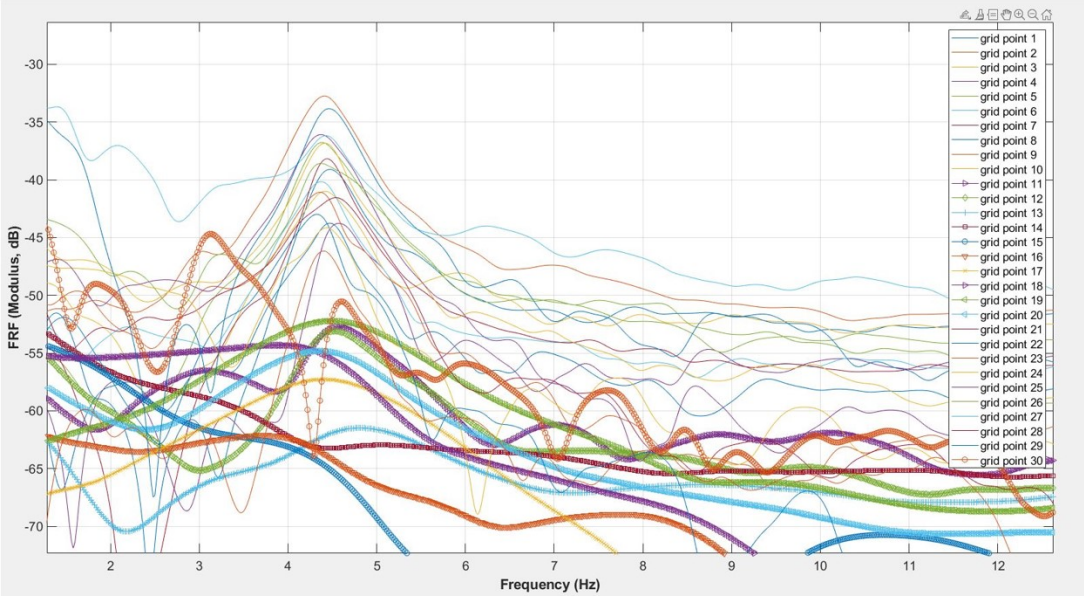


Figure 4.20.: FRF amplitude close to Mode 1

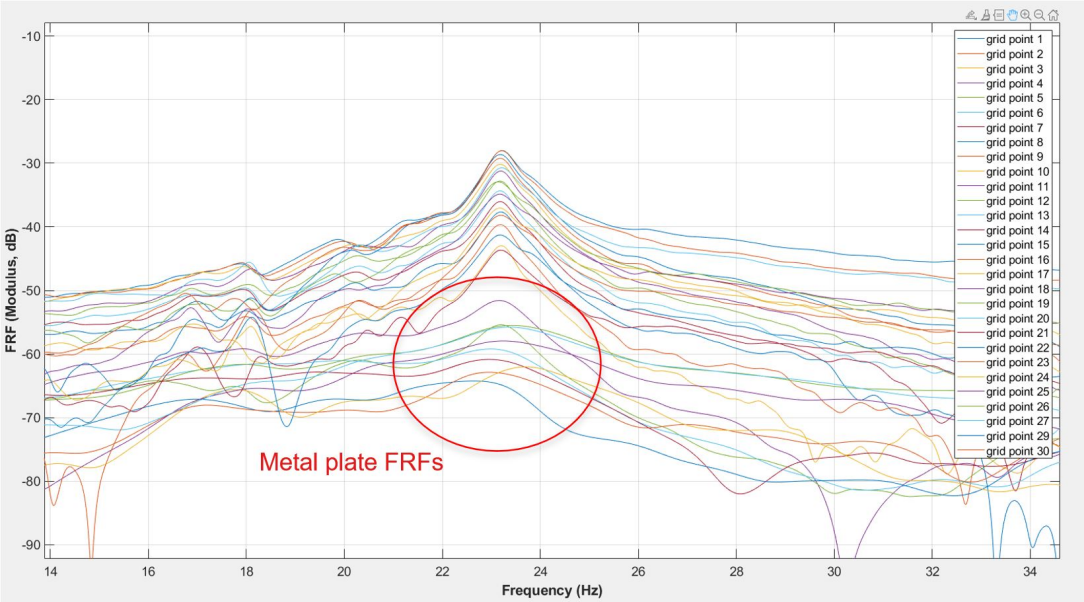


Figure 4.21.: FRF amplitude close to Mode 2

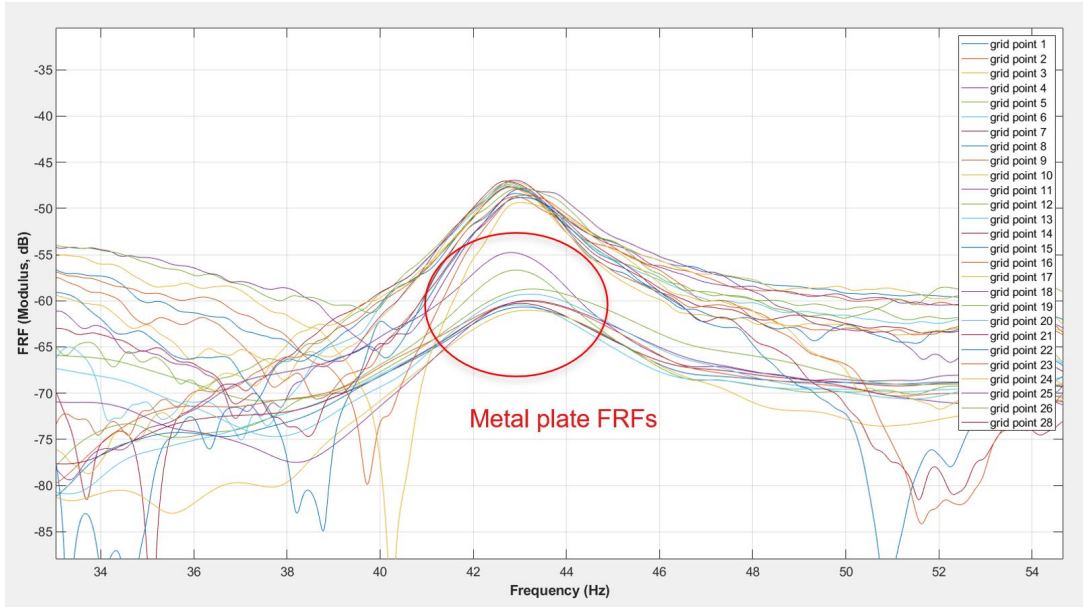


Figure 4.22.: FRF amplitude close to Mode 3

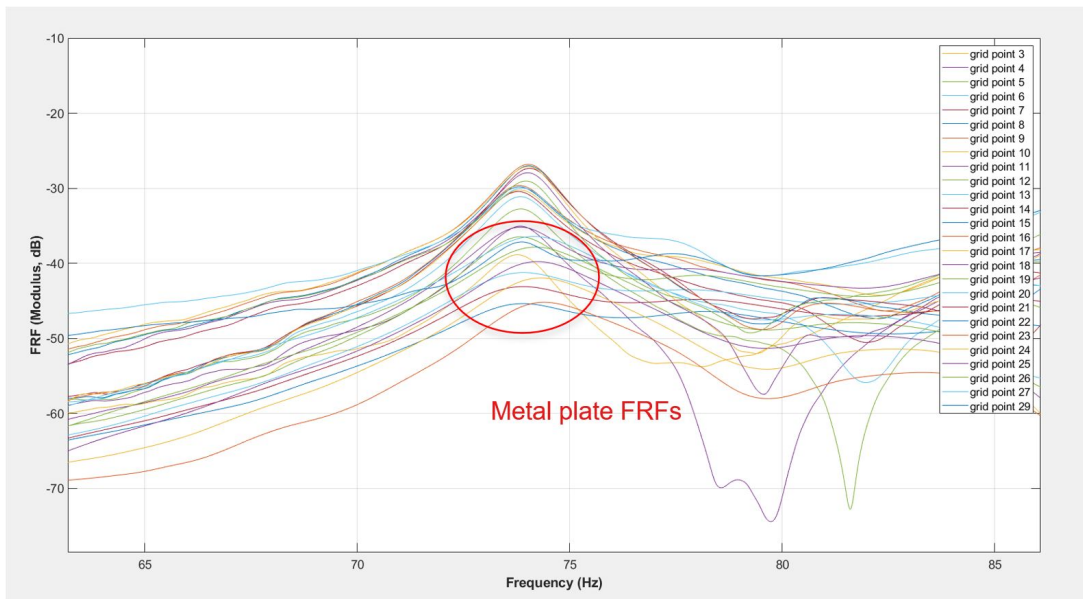


Figure 4.23.: FRF amplitude close to Mode 4

The 3 resulting mode shapes, after scaling the amplitudes from -100 to 100 are shown in Figure 4.24-Figure 4.26, and they all appear either symmetric or anti-symmetric.

4. Experimental Modal Analysis: Radar Antenna

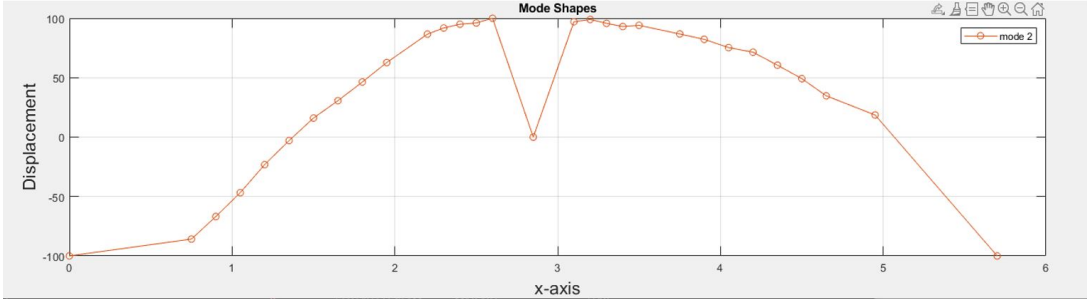


Figure 4.24.: Mode Shape 2 at 23 Hz

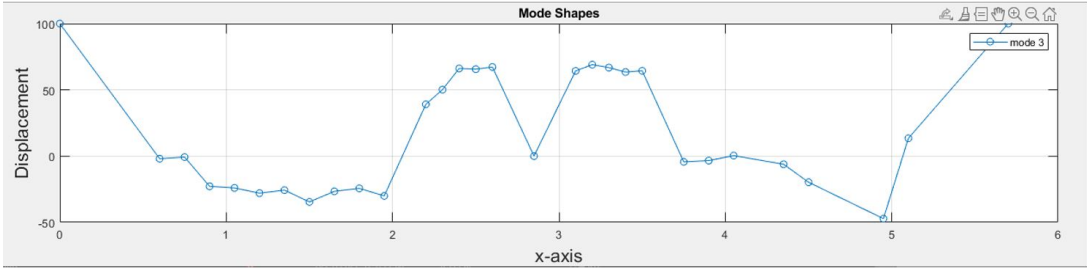


Figure 4.25.: Mode Shape 3 at 44 Hz

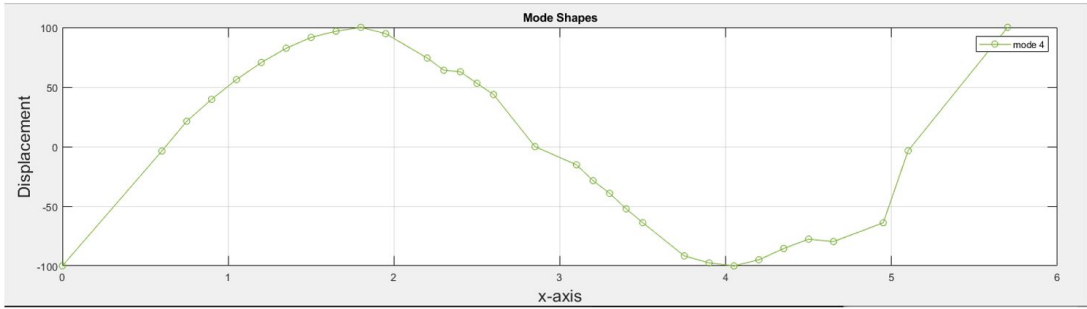


Figure 4.26.: Mode Shape at 74 Hz

4.5. Conclusions

The application of [EMA](#) on the radar antenna provided significant information for its dynamic characteristics under idle conditions, thus providing important input for the investigation of what a long-term sensor network set-up, under operational conditions, could look like. In short:

- The acceleration amplitudes and the structure's frequency response allow the careful prediction of the appropriate sensor specifications.
- The identification of measurement points that do not correspond to nodes of zero displacement ensures an appropriate future sensor placement.
- The apparent reciprocity of the antenna system demonstrates a linear structure response (for idle conditions).
- The failure to get vibration response from the y direction of the radar leads to the avoidance of sensor placement in this area.
- The identified natural frequencies ([Table 4.5](#)) and its respective mode shapes can be used to further improve the Finite Element model that has been developed.

Later in [Chapter 6](#), further investigation on how these results, in combination with results from [Chapter 5](#) and a critical look on existent bibliography, can support the proposal of a suitable sensor network under operational conditions.

Table 4.5.: Summary of the radar antenna's natural frequencies

Mode	Natural Frequency (Hz)
1	4,5
2	23
3	44
4 (plate)	74
5 (plate)	174

5. Operational Modal Analysis: Mast

5.1. Experiment objective

In [Chapter 1](#), it was mentioned that installation of nautical radars are planned on masts standing on top of offshore substations. This fact brings into focus the interaction of the nautical radar with the mast. The mast is affected by environmental loading that causes vibrations that are also shared with the nautical radar system. By examining the dynamic properties of such a structure, it can be assessed how the mast response affects the response of the nautical radar. Since the mast is a large structure, conventional actuators like an impact hammer, can not transmit enough energy all across its height. That's where the role of *OMA* comes into play, where known input forces are not needed in order to identify a system's structural characteristics. As already discussed in [Chapter 1](#) and [Chapter 3](#), by employing this output-only method, one can perform vibration measurements relying only on environmental loading.

5.2. Structure description

The steel structure at hand ([Figure 5.2](#)) is of triangular shape, with a resulting height of 20.01 m. It consists of 3 main columns, that are mounted to the ground on a concrete slab ([Figure 5.2a](#), and they are connected through diagonal bracings. Floor grating exists in each one of the bays, while a ladder in the middle ensures access to them ([Figure 5.2b](#)).

5.3. Experiment design and mast Instrumentation

Since the available equipment is the same that was used for the radar measurements, opportunities for a sophisticated sensor network, with distributed sensors across the mast's height were unachievable. With the available DAQ (4 output channels) and accelerometers, simultaneous ambient measurements could be performed only on one of the bays.

FEM by [Sfetsios \[2022\]](#) showed that the first two modes are strictly bending modes. The identified modes are presented in [Table 5.1](#). It's respective shapes are shown in [Figure 5.3](#).

Table 5.1.: First two natural frequencies of the mast

Mode No.	Freq. (Hz)
1	2.87
2	4.41

5. Operational Modal Analysis: Mast

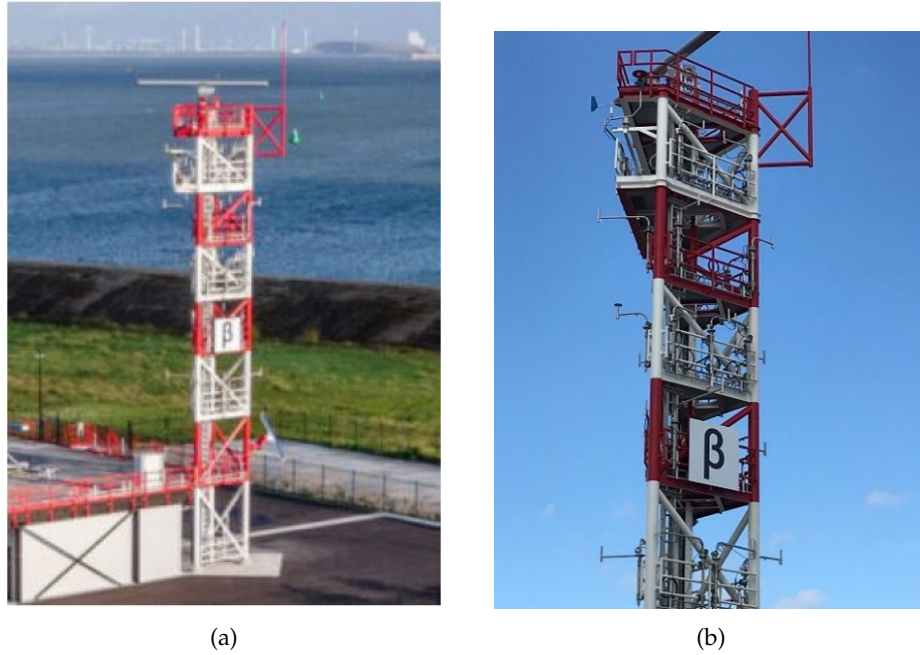


Figure 5.1.: Different views of the mast

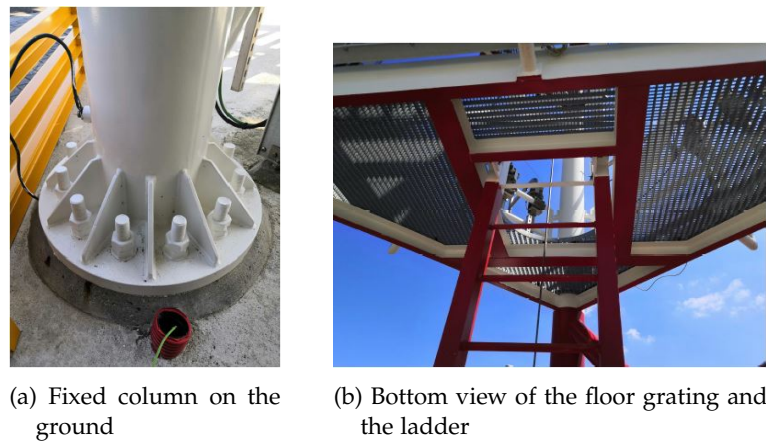


Figure 5.2.: Mast elements

By taking the above into account, two sets of tests were devised. One test with the goal to capture the bending mode in the x-direction and one to capture the bending mode in the y-direction. The established axis system is shown in [Figure 5.4](#). The preferable floor for the vibration measurements is the next to last floor for two main reasons. Firstly, this is the floor where the column elements of the structure end. Since the columns are the only continuous element from the ground to the top of the mast, they pose the most preferable sensor locations. Secondly, the largest responses of the structure are expected on the top of it, thus making the most desirable measurement location.

5.3. Experiment design and mast Instrumentation

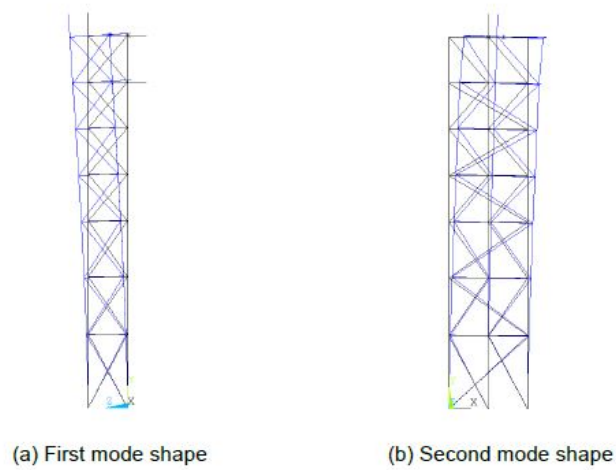


Figure 5.3.: First two bending modes from Vasilis' finite element model [Sfetsios \[2022\]](#)

Apart from the attempt to capture the two bending modes, the aforementioned strategy aims also to reveal any other existent modes, possibly local and in higher frequencies, that can also lead to conclusions about the the mast's response in its top floor, which is directly intertwined with the response of the radar antenna.

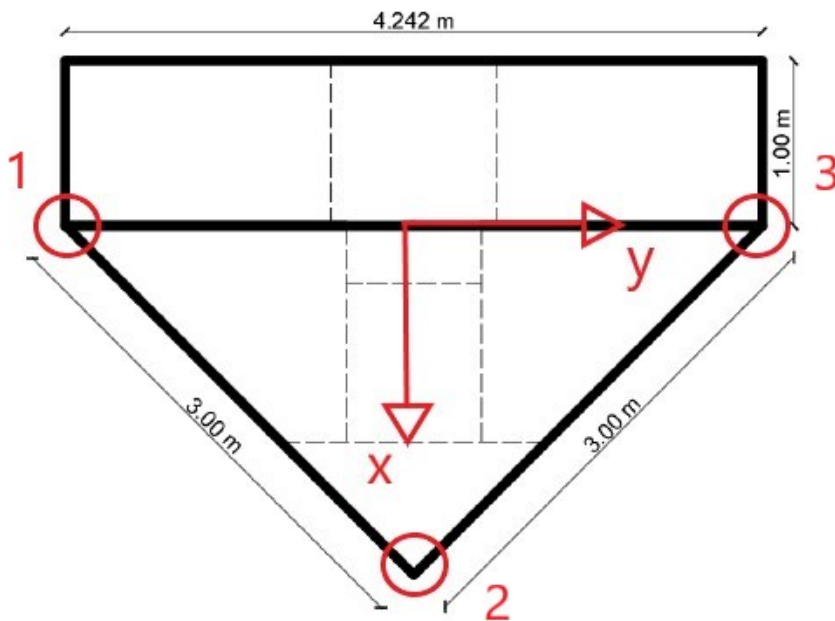


Figure 5.4.: Mast axis system along with the numbering and location of the its columns

The sensors were placed at the cumulative height of 19,05 m. During the first set of tests, 3

5. Operational Modal Analysis: Mast

Table 5.2.: Measuring equipment for the mast vibrations tests

Equipment name	Measurement range	Sensitivity	Frequency range	Channels (columns)
PCB_352a24	50 g pk	100 mV/g	1-10000 Hz	1
PCB_356a44	100 g pk	50 mV/g	0,7-7000 Hz	3
PCB_356a45	50 g pk	100 mV/g	0,7-7000 Hz	2

accelerometers were placed in the 3 respective columns parallel to the y-direction, while for the second set, parallel to the x-direction. The sensors used, along with their respective column placement are presented in Table 5.2. Figure 5.5 shows how the measurements points were distributed across column No. 1. For each set of tests, two-minute samples were taken as they were deemed enough to capture vibration periodicity, at three different sampling frequencies (1, 2 and 10 kHz). The experiments lasted two days, with the temperature levels at around 10 °C, and a mean wind of 3 Beaufort.



Figure 5.5.: Measurement points in column No. 1

5.4. Methodology and Results

The approach taken for the mast measurements aims not only to identify and cross-examine the modal analysis results from the Finite Element analysis, but also to provide information on any existent modes that could affect the radar antenna's resonant response. In order to achieve that, the combination of two Operational Modal Analysis techniques are employed, as already described in Chapter 3. The Natural Excitation Technique, that uses the cross-correlation function of the signals in order to translate the white noise excitation into

free vibration data and the Eigensystem Realization Algorithm that facilitates the acquisition of a numerical model of the system, that in return used to obtain the modal characteristics of the system (the natural frequencies and damping ratios). The methodology to achieve this task is the following:

1. Estimation of cross-correlation function to get the Impulse Response Function (time-domain) for each output by choosing a reference channel (NExT)
2. Determination of model order, rows and columns in Hankel matrix (ERA)
 - no. rows \geq model order
 - no. columns = enough to cover the decaying section of correlation function
3. Stabilization diagram and Modal Assurance Criterion (MAC)
4. Natural Frequency identification

Modal analysis in the y-direction

The sampling frequency eventually used for the realization of the results was 1 kHz. Since the distinguishable natural frequencies of the radar were all below the 200 Hz mark, the results presented from hereinafter are concentrated in the frequency range of 0 to 200 Hz.

Before starting the system identification procedure, the cross-spectral density between channels 2 and 3 were created in order to determine the clean peaks that were visible within the spectrum. For the spectral density estimation Welch's method was used, with its parameters shown in Table 5.3. Evident from the peaks in Figure 5.6 is the existence of a significant number of possible natural frequencies.

Table 5.3.: Welch's method parameters (y-direction)

Sampling Frequency	1000 Hz
Window	Hanning
Segments	10
Overlapping factor	0.5

Next follows the setting of some of the NExT parameters in order to extract the Impulse Response Functions, which are used as free vibration data for the ERA. Channel 2 is used as reference for the estimation of the three cross correlation functions in the time domain, as it is the one with the biggest amplitude. According to Derrick [2004] a good choice of number of lags in the cross correlation function is half the number of the data of time signal. The 2-minute time signal with a sampling frequency of 1 kHz results in a number of data $N_{data} = 120.000$ making the number of lags equal to 60.000. By taking these into account, the three resulting Impulse Response Functions are visible in Figure 5.7.

In order to move forward to the estimation of the system's modal parameters through the ERA, it is required to choose the dimensions of the Hankel matrix. As mentioned previously in Chapter 3, the number of columns should cover the decaying section of the correlation function. In this particular set of cross-correlation function (or Impulse Response Function (IRF)) this number was 6000. Since the model order is unknown, a stabilization diagram was used in order to avoid unnecessary truncation of the singular values. In any case, the

5. Operational Modal Analysis: Mast

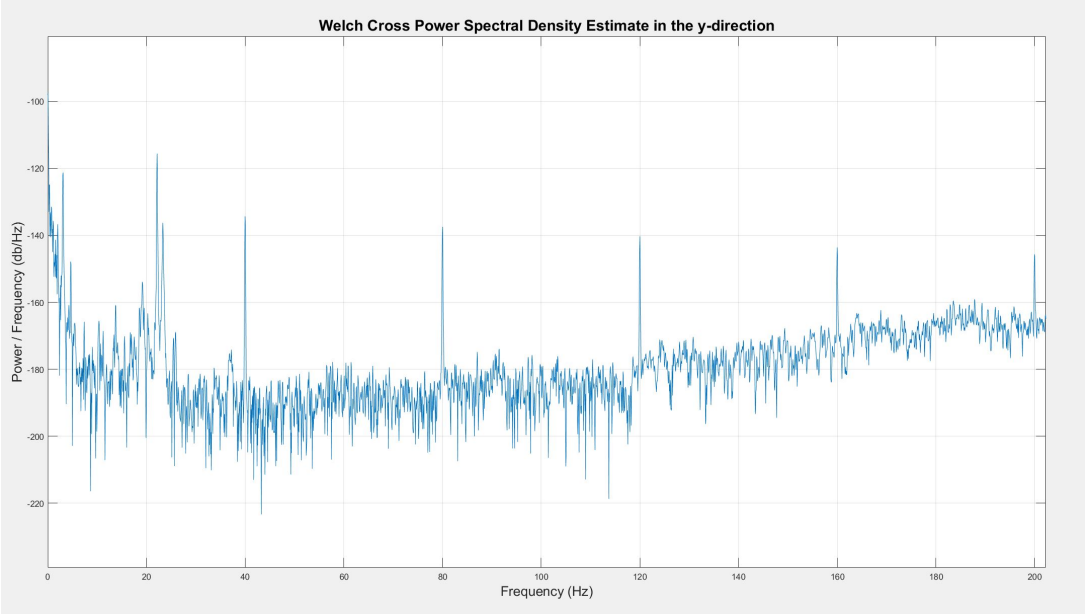


Figure 5.6.: Cross Spectral density of channel 2 and 3 (y-direction)

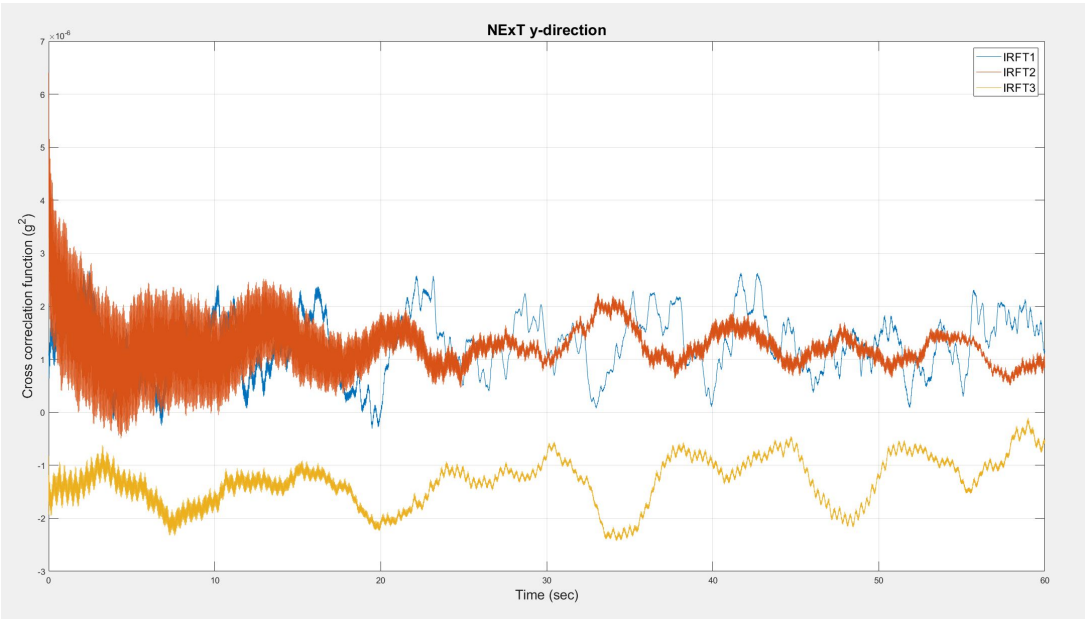


Figure 5.7.: Impulse Response Functions for the y-direction (reference channel = 2)

number of rows should be greater or equal to the model order. The resulting parameters were chosen through an iterative procedure and are shown in Table 5.4.

To distinguish the real from the numerical modes, two thresholds were used. According to Caicedo [2011], modes with a damping ratio below 5% and Modal assurance criterion (MAC)

Table 5.4.: Hankel matrix and truncation parameters (y-direction)

No. columns	6000
No. rows	500
Model order	300

values below 90% should be discarded. The resulting stabilization diagram for the ERA on the y-direction is presented in Figure 5.8. As it can be shown, there are six modes that are identified in a stable way, marked by the fainted black line. Apart from the stabilization diagram the figure shows how the identified modes fit with the cross spectral density of the signal. The results of the identification are summarized in Table 5.5.

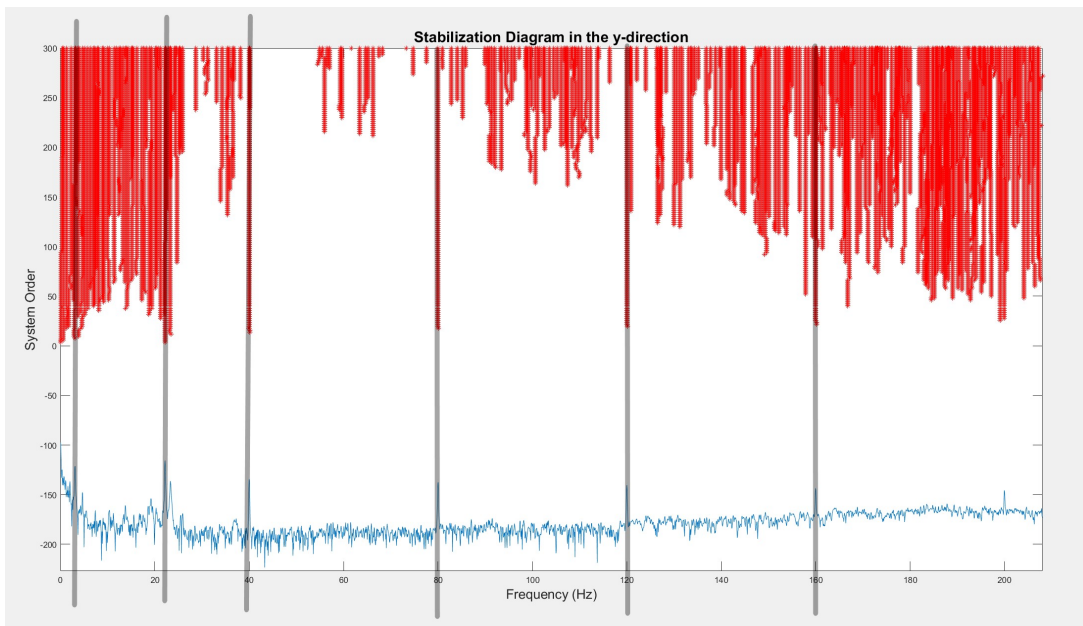


Figure 5.8.: Stabilization Diagram – y-direction

Table 5.5.: Identified modal properties for the y-direction

Mode	Nat. Freq. (Hz)	MAC (%)	Damping (%)
1	3	90	0.8
2	22	100	0.3
3	40	99	0.1
4	79	99	0.1
5	120	99	0.02
6	160	99	0.01

5. Operational Modal Analysis: Mast

Modal analysis in the x-direction

The sampling frequency used for the realization of the results for the x-direction was 2 kHz. Again the results are shown for the first 200 Hz of interest. The cross-spectral density parameters are shown in Table 5.6. Evident from the peaks in Figure 5.9 is again the existence of a number of possible natural frequencies.

Table 5.6.: Welch's method parameters (x-direction)

Sampling Frequency	2000 Hz
Window	Hanning
Segments	10
Overlapping factor	0.5

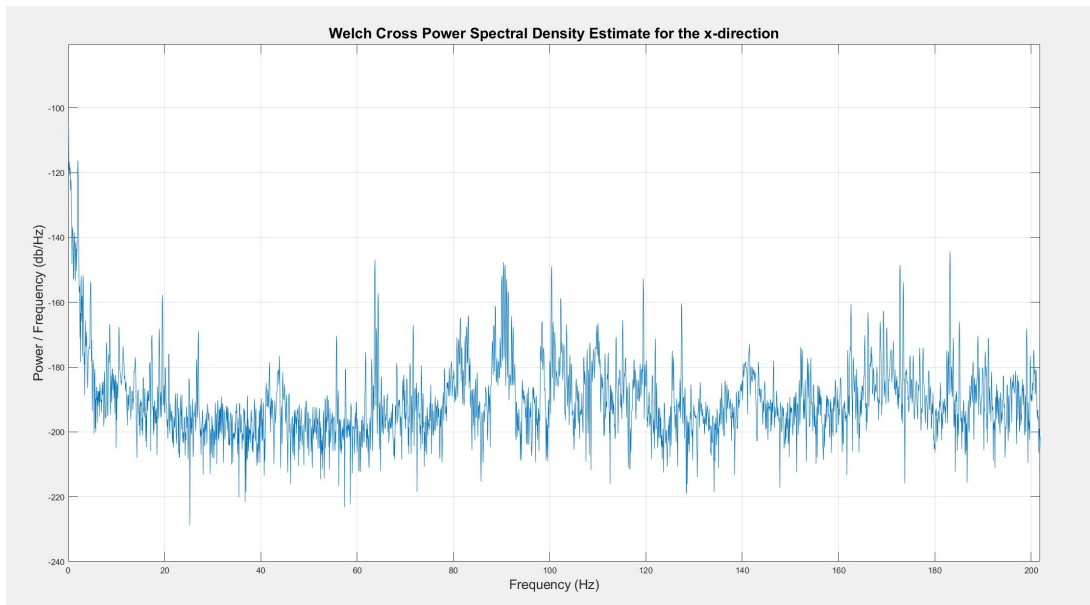


Figure 5.9.: Cross Spectral density of channel 2 and 3 (x-direction)

For the implementation of `NExT` Channel 2 is used as reference for the estimation of the three cross correlation functions in the time domain, as it is the one with the biggest amplitude. The number of lags is estimated with the same principle for the y-direction, resulting in a number of 120000. The three resulting Impulse Response Functions are visible in Figure 5.10.

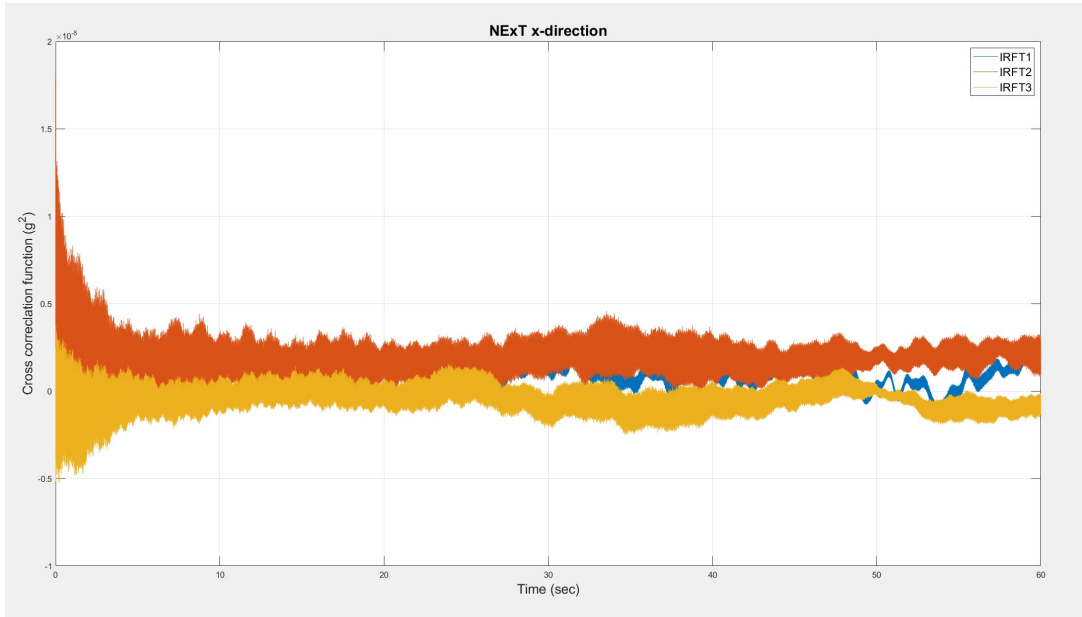


Figure 5.10.: Impulse Response Functions for the x-direction (reference channel = 2)

The resulting parameters for the Hankel matrix were chosen through an iterative procedure and are shown in Table 5.7.

Table 5.7.: Hankel matrix and truncation parameters (x-direction)

No. columns	5000
No. rows	700
Model order	300

The same principles were chosen to distinguish the real from the numerical modes. The resulting stabilization diagram for the ERA on the x-direction is presented in Figure 5.11. As it can be shown, there are 3 modes that are identified in a stable way, marked by the fainted black line. Apart from the stabilization diagram the figure shows how the identified modes fit with the cross spectral density of the signal. The results of the identification are summarized in Table 5.8.

5. Operational Modal Analysis: Mast

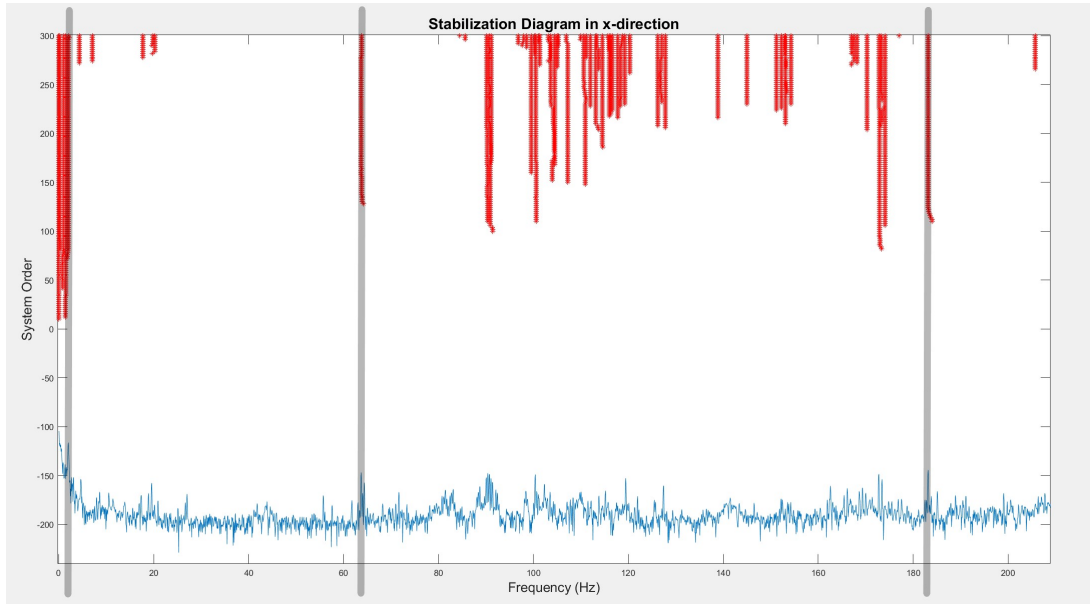


Figure 5.11.: Stabilization Diagram – x-direction

Table 5.8.: Identified modal properties for the x-direction

Mode	Nat. Freq. (Hz)	MAC (%)	Damping (%)
1	2	98	2
2	63	95	0.1
3	183	93	0.05

5.5. Conclusions

The Operational Modal Analysis on the mast showcased some of the dynamic characteristics of the structure. Though the limited nature of the equipment does not allow to say a lot about the mode shapes of the mast, the identified natural frequencies of the mast's top floor can help evaluate what kind of vibrations are shared with the radar antenna.

Immediately noticeable from the vibration results, is the fact that the first two identified natural frequencies from OMA are coinciding in direction and mode order with the ones from FEM (Table 5.9). If it is also taken into account that the FEM analysis contains a number of assumptions and simplifications, then the identified frequencies from OMA could indeed belong to the first two modes of vibrations of the mast. This outcome, on the one hand it preliminary cross-validates both approaches and on the other hand, can further facilitate the update of the FEM model.

Table 5.9.: Comparison between natural frequencies from FEM and OMA

	FEM	OMA
1st Natural frequency (x-direction)	2.87 Hz	2.01 Hz
2nd Natural frequency (y-direction)	4.41 Hz	3.04 Hz

Another deduction that can be made from this analysis is the fact that there is a number of mast modes that its natural frequencies are really close to the natural frequencies of the radar antenna. By taking a look at the summary Table 4.5 in Chapter 4 and the summary Table 5.10, it is apparent that the 2nd mode of the mast is really close to the 1st mode of the radar antenna (3 Hz and 4,5 Hz), and that the 3rd identified mode of the mast (as presented on Table 5.10) is close to the 2nd of the antenna (22 Hz and 23 Hz). Since it is a coupled system, excitation frequencies between the closely spaced modes, could amplify the response of the antenna by a significantly large margin, further contributing to the antenna's instability and in return to the fatigue accumulation, when excited close to resonance.

Finally, it becomes noticeable that responses at higher frequencies exist (higher than expected just from wind excitation which is normally low frequency), leading to the conclusion that energy may be transferred locally between different modes, and making resonant frequencies beyond the wind's frequency range observable.

Table 5.10.: Summary of mast modes for both examined directions

Mode	Natural Frequency (Hz)
1 (x)	2
2 (y)	3
3 (y)	22
4 (y)	40
5 (x)	63
6 (y)	79
7 (y)	120
8 (y)	160
9 (x)	183

In the following chapter, it is examined how the mast response is correlated with the radar's response and how the products from the modal analysis on the mast can be further utilized on any future long-term vibration measurement campaign on the radar antenna.

6. Future radar monitoring system proposal

This chapter focuses on how the results obtained from the [EMA](#) on the radar antenna and the [OMA](#) on the mast can be employed in order to facilitate vibration measurements on the radar antenna under operating conditions. First, a discussion on the most fitting monitoring and system identification methods takes place. Then it is investigated how the added rotation of the antenna would affect a vibration measurement campaign and its results. Lastly, a suitable sensor network set-up is introduced. What needs to be remarked at this point is that all the following deductions and proposals are valid only in the case that a nominally identical radar will be used for the vibration-based monitoring.

6.1. Structural Health Monitoring and System Identification

Structural Health Monitoring ([SHM](#)) is defined as the use of in-situ, nondestructive sensing and analysis of structural characteristics, including the structural response, for the purpose of estimating the severity of damage and evaluating the consequences of damage on the structure in terms of response, capacity, and service-life ([Guan \[2006\]](#)). Maintaining the continuous performance of the radar depends highly on monitoring the occurrence, formation and propagation of damage. So, what is needed is an efficient method to accumulate and evaluate structural data, in order to assess structural damage and make decisions on the radar's structural health.

This thesis is focusing on how the above can be achieved by performing a long-term vibration-based structural health monitoring. The basic approach of vibration-based damage detection is to monitor changes in the dynamic properties of a structure by comparing dynamic parameters between a baseline or undamaged state and a damaged one ([Karbhari \[2009\]](#)). This damage identification process can be realised by either employing physical model based techniques or data-driven techniques. Since the physical properties of the radar antenna are mostly unknown, results can be obtained by utilizing data-driven methods that rely on the use of dynamic features such as the modal shapes, frequencies and damping ratios, in order to perform a comparison between different structural states. Since the radar is relatively new, it can be assumed that it is currently under a pristine structural state, which can therefore be considered and used as baseline state.

By considering this data-driven approach, what comes to the forefront of the discussion is how to acquire these structural dynamic properties through vibration measurements, by also taking into account environmental conditions and measurement campaign restrictions. In any forthcoming project plans, the radar antenna will be positioned on a limited access environment (either on top of a mast or on a specially designed wind turbine platform) and under environmental loading by wind among other indirect loading by the coupled structure that rests upon. And all these, while the radar itself will be under operational

6. Future radar monitoring system proposal

conditions (rotating antenna). As mentioned already in previous chapters, such a problem can be dealt with by applying Operational Modal Analysis and the *SI* methods that come with it, a modal analysis that relies only on ambient environmental excitation in order to define modal parameters.

A wide variety of vibration-based health monitoring systems have been developed through time. What is of importance in selecting an appropriate damage detection method is to define certain environmental, structural and equipment limitations as reported below:

- Environmental conditions and structure size dictate the kind of modal analysis (input-output/output-only).
- Available or obtainable structural and dynamic characteristics of the structure dictate the method of damage detection (Parametric vs. non-parametric methods)
- Number of available sensors/measurements locations also dictate if global or local damage information can be obtained

Das [2015] reviewed a wide variety of vibration-based damage detection techniques. Parametric modal-based methods (relating damage to dynamic modal parameters like mode shapes, stiffness, mass etc.) such as the frequency response or strain energy methods were proven successful for low vibration modes, but mainly relied on stiffness loss for accurate results, a parameter unknown for the radar antenna, while the mode shape method (curvature mode), examined by Lestari [2007] employs the same parameter. Miguel [2012] employed a combination of output-only *SI* techniques and the harmony search algorithm to perform a damage identification on a beam, but relied on numerical and FE models, associating damage to stiffness loss as well. Yin [2009] used the same modal identification method present on this thesis (*NEXt* and *ERA*), and then utilized the dynamic reduction based damage-detection method. With a small number of sensors he succeeded in detecting structural damage by calculating equivalent stiffness loss. Gul [2008] employed an output-only parametric damage detection method, where ambient vibration data were used to compose the unscaled modal flexibility matrix and extract in return the deflection profile of both a laboratory steel grid and a bridge. All of the aforementioned parametric damage detection methods have been dealt by researchers with a similar approach that could be well represented in Figure 6.1. A common element of these methods, and a potential drawback for the radar antenna case, is that they usually are accompanied by a robust *FEM* or numerical model as means of verification. Although such an antenna model exists, it is governed by assumptions on material and dynamic properties, and using parameters such as stiffness to accurately identify damages can prove a challenging task. However current *FEM* model can significantly assist in developing structural damage scenarios, as well as identifying local structural damage locations, which affect only higher frequency modes and may prove difficult to identify using output-only methods.

A plethora of non-parametric damage detection methods (based on probabilistic models that extract damage information directly from the measured accelerations) were also subject of research. Das [2015] explored the bayesian probabilistic interference, in which he firstly identified the modal parameters and the uncertainties and in the next step, he measured the probability of the reduction in stiffness, considering a damage threshold. Auto-regressive models, are widely used as a non-parametric approach (Gul [2009], Magalhaes [2011], Carden [2008]) but they prove effective when based on structural parameters like mass or stiffness. Kopsaftopoulos [2010] reviewed the output-only Power Spectral Density (*PSD*) method

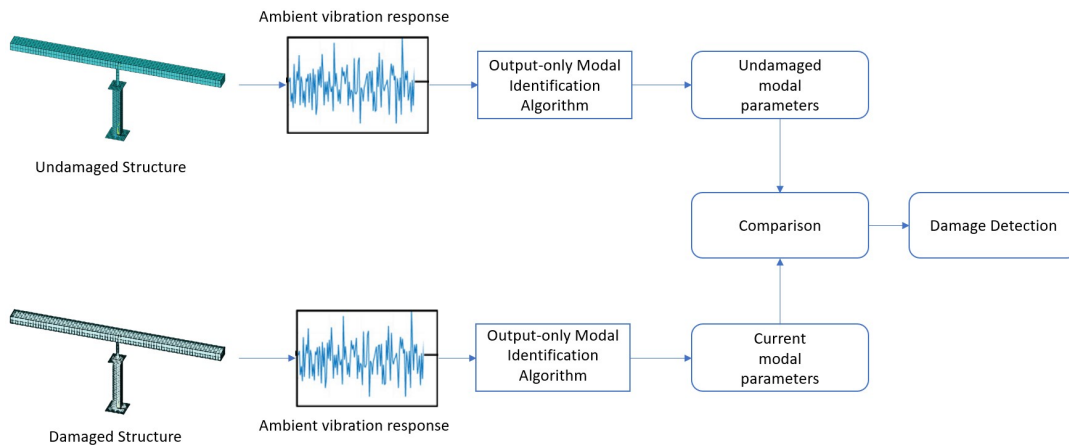


Figure 6.1.: A schematic of output-only parametric vibration-based damage detection methods as described at Avci [2020]

on a truss tower, resulting in successful damage detection once certain damage types/scenarios are determined, making it an appealing technique for the radar antenna case.

As showcased above, although a large number of damage detection methods can be applied to assess damage on the radar antenna, damage assessment may prove a demanding assignment if physical parameters or accurate FEM models are not employed. As the current case study is based on data-driven features, what could prove beneficial would be to utilize Machine Learning (ML) techniques which are “data-hungry” and rely on black-box models, whose parameters are dictated by a large number of observations. A review by Avci [2020], introduces ML-based methods that simply involve two tasks: dynamic feature extraction and classification, which makes the ML-based methods more generic and advantageous than non-ML based methods in vibration-based structural damage detection in structures. By extracting dynamic properties such as natural frequencies and mode shapes from OMA and classifying any input with the use of Artificial Neural Networks, the structural integrity of the radar can be assessed. Since ML techniques are quite complex and out of the scope of this study, further investigation on the applicability of such methods is to be performed by any future researcher.

6.2. Operational and environmental conditions

In order to design a robust sensor network that can provide all the necessary dynamic characteristics for developing a vibration-based damage detection method, one has to consider all the operational and environmental conditions. In this section it is examined how these conditions may affect long-term measurements and how the modal analysis performed in the current study may facilitate to overcome certain obstacles set by them.

6. Future radar monitoring system proposal

A long-term vibration campaign for the radar, under operating conditions, will be governed by excitations from the following sources:

- Wind
- Rotation of the radar antenna
- Mast movement
- Humidity
- Temperature

It is expected that the radar antenna will be loaded by wind. One common problem of [OMA](#) techniques - which as explained should be the primary modal analysis method to be used, given that antenna will be under operating conditions - is the unknown input loading, which at times may include harmonic forces and not fulfill the Gaussian white noise excitation basis. In general wind loads approximate this broadband random excitation, but harmonic components may well appear during specific measurement periods. This means that harmonic modes may be mistaken for being structural modes. Although there are [SI](#) approaches in literature that could possibly counter such a phenomenon, including the [ERA](#), these harmonics frequencies must be known a priori ([Gasparis \[2019\]](#)). Since though the first natural frequencies of the radar antenna are already extracted from the [EMA](#) campaign, distinction between a harmonic and structural mode becomes a simpler task. Especially in the case that a large [OMA](#) data-set, during different wind conditions, is accumulated.

Another form of excitation of the radar antenna will come through the rotation of the antenna itself. When in operating conditions, the radar antenna rotates with a steady velocity of 20 rpm (0.3 Hz). Through widespread studies on wind turbines, it is observed that the tower vibration measurements are characterized by peaks at the rotational frequency and the harmonics of the nacelle blades [Chauchan \[2011\]](#). Such a characteristic may also be prevalent on the radar measurements, where the rotational frequency of antenna and its derivatives might appear. These frequency peaks are usually associated with thick tails which may mask the structural dynamics of the radar antenna if they appear in the neighbourhood frequencies. With the assumption that the rotational speed threshold, where dynamic properties of the structure are altered, is not surpassed (very low rotational speed), the natural frequencies already identified by the [EMA](#) can assist to tackle this "masking" problem. Once these rotational harmonics are identified, they can be removed by Kurtosis techniques followed by linear interpolations before the estimation of modal parameters ([Damgaard \[2011\]](#)).

The other significant excitation force that will contribute to the radar loading is the mast movement. On the one hand, mast movement constitutes another steady-state broadband random excitation, as it will be loaded by wind as well. On the other hand, in case the mast is located in offshore conditions where wave loading can be also dominant, noise and harmonic contributions are introduced and may affect the system identification. Again, by taking into advantage the already identified dynamic properties acquired through the [EMA](#) on the radar and the [OMA](#) on the mast, any future researcher can use the known frequency peaks in order associate any other peaks in the spectral density with the environmental loading.

Lastly, the environmental effects of humidity and temperature should not be overlooked. Changes in the natural frequencies and mode shapes are usually associated with changes in the temperature and humidity. Therefore it is important to eliminate such factors, especially

when trying to estimate damages, which are also identified by small changes to modal parameters.

As documented from the above, extraction of dynamic properties from ambient measurements is a demanding task. Varying environmental and operating conditions affect measured signals and can often mask small changes in the system's vibration data that may have been caused by damage. A combination of large number of observations and utilization of the already defined dynamic properties must take place in order to detect structural damages. [Sohn \[2007\]](#) introduces an extensive review of novel approaches on how dynamic data can be normalized and used efficiently for the health monitoring of structures.

6.3. Sensor network proposal

6.3.1. Wireless Sensor Network

What needs to be established first in order to design a robust sensor network is how the sensors are connected to the central data acquisition system. Since the radar antenna will be under operational conditions during any future measurement campaign, with constant rotation on the horizontal plane, cable-based solutions are limiting, leaving only two possible means of connection, either with slip rings or wireless. Since slip rings constitute an expensive solution, difficult to be realized under offshore conditions, a Wireless Sensor Network (*WSN*) poses as the sole solution. Wireless sensors reduce significantly the installation time and costs, and are not subjected to wear or breakage of wires.

Wireless sensor networks for structural health monitoring have been widely applied in civil structures in the past. Of most interest are various publications of M. J. Whelan. In [Whelan \[2009\]](#), he monitored a highway bridge, where a real-time streaming of 40 channels of measurement data sampled at an effective rate of 128 Hz per sensor for ten test durations each exceeding three minutes was successfully achieved. In [Whelan \[2010b\]](#), he performed vibration measurements with wireless sensors on a prestressed concrete bridge with operational modal analysis. He aimed to use the results from *OMA* in order to develop a *FEM* model, concluding that there was a difference in the range of 10% between *FEM* results and the ones obtained from the wireless acceleration signals.

A series of parameters and limitations need to be considered when choosing a *WSN*. Initially, the data storage and transmission scheme needs to be established. According to another study of [Whelan \[2010a\]](#), wireless networks have generally relied on either local data logging and post-sampling transmission or on low sampling rates and/or limited numbers of sensors in order to address transceiver bandwidth limitations for live monitoring. Such a choice needs to be made by the researcher according to the needs of the modal analysis. An additional parameter to be determined is the TS protocol [Bocca \[2011\]](#). TS protocol ensures that the synchronization error among all mounted sensors should be always below 10 μ s.

6.3.2. Sensor specifications

From the beginning of the experimental campaign on the radar antenna it became apparent what kind of equipment specifications are appropriate for performing vibration measurements on the radar. As reported on the results on [Chapter 4](#), it is evident that all the first

6. Future radar monitoring system proposal

modes of vibration were able to be extracted with a 50 g accelerometer. There were times though, usually when the hammer impacts were too close to the sensor, that the recorded acceleration amplitudes were well above the 50 g mark and closer to 100 g, causing the signal to be clipped. Although such a result could lead to the conclusion that an accelerometer with a measurement range of ± 100 g is the most fitting one, this would also mean that most of the times the dynamic range of the sensor would not be the most convenient one, leading to a bad signal-to-noise ratio. One way to compromise between good dynamic range and capturing of higher acceleration levels, is to place 100 g accelerometers on the edges of the structure (where acceleration levels are commonly bigger) and 50 g ones closer to the joint of the antenna.

Another important specification to consider are the measurement axes. As it was evidenced from the [EMA](#) measurements, vibrations cannot be transmitted in the y direction, due to the material properties on the sides of the antenna. What could be of use then is tri-axial accelerometers, that can estimate vibration levels also on the y and x directions.

The frequency range of the used accelerometer was 1-10000 Hz. The results were inconclusive on the higher frequency end, since possible high modes of vibrations were indistinguishable after the 200 Hz mark. It can be assumed that the value of 10000 Hz is good enough to capture the frequencies of importance. As far as the lower end is concerned, the lower natural frequency identified was at the level of 4,5 Hz, making the 1 Hz mark suitable for the radar antenna case.

Lastly, the sampling ratio of the Data Acquisition System should be determined according to the wireless sensor transmitting limitations, as reported above, and the sampling frequency rule of thumb (sampling frequency should be 10 times higher than the highest excited frequency).

6.3.3. Sensor placement

One of the most important facts that concerns the sensor placement is to avoid modal nodes. A measurement point cannot be located at the node of a mode otherwise that mode will not be seen in the frequency response function and in return in the mode shape. Evident from the FRFs from the 3 clear modes presented in [Chapter 4](#), is the fact that none of the measurements points was a modal node, since a peak was present for every single FRF all across the natural frequencies. This means that all measurement points can be used in the future as an output channel point in the z-direction.

Since the number of wireless accelerometers that can be placed on the radar is dependent on the budget which is unknown, some arbitrary possible set-up configurations can only be proposed. All measurements points used for the experimental tests in Stellendam can be a potential output channel point. However, it should be taken into account that the number of accelerometers installed should not modify the weight of the structure significantly, because the dynamic response of the structure would then be altered.

Since damage assessment constitutes the main scope of any further research, the additions of strain gauges in specific areas can further facilitate the health monitoring process and help identify local damages, which may be difficult to be detected from the vibration-based damage detection algorithms. From [Sfetsios \[2022\]](#) Finite Element study on the radar antenna, it became apparent that there are sections where stress concentration is significantly

higher than others Figure 6.2. These areas are the ones mainly considered for strain gauge placement.

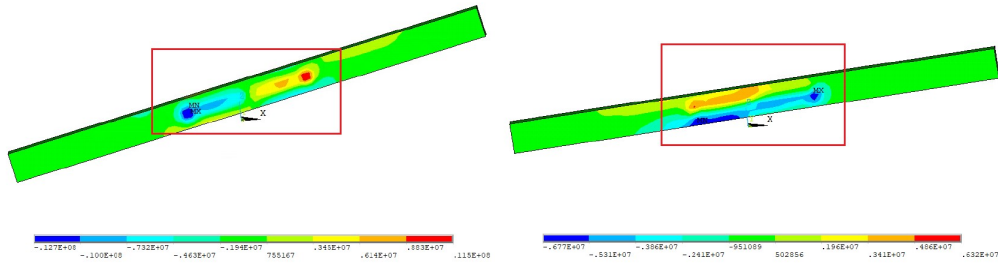


Figure 6.2.: Stress concentration from fatigue damage accumulation in FEM

By taking into account all the mentioned parameters and criteria in this chapter, the next two figures suggests possible configurations with both accelerometer and strain gauge placement (Figure 6.3, Figure 6.4). As strain gauge characteristics and placement were not part of the current study, a comprehensive research, including the investigation of damage type scenarios, should be carried out in order to validate the proposed strain gauge arrangements.

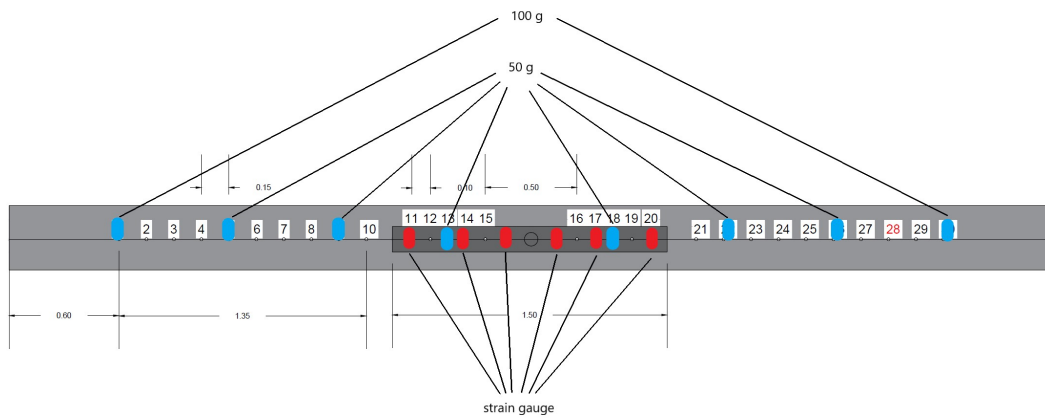


Figure 6.3.: Proposed sensor network configuration 1: 8 accelerometers and 6 strain gauges

6. Future radar monitoring system proposal

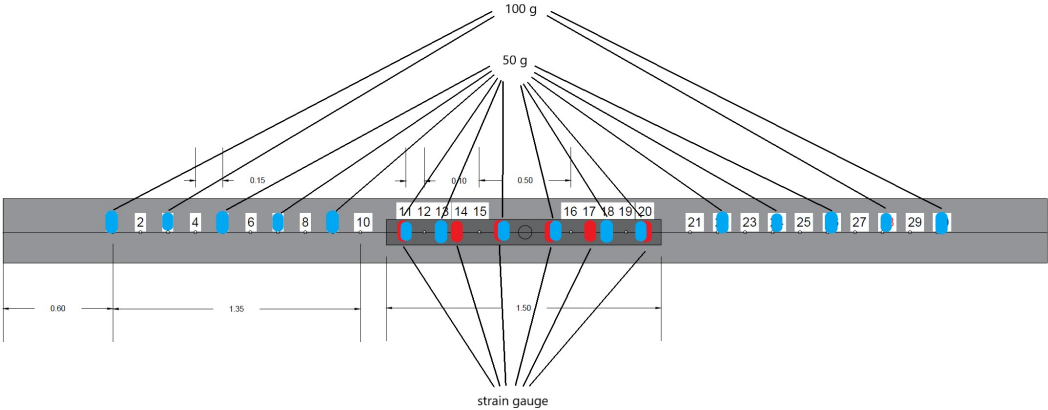


Figure 6.4.: Proposed sensor network configuration 1: 16 accelerometers and 6 strain gauges

7. Conclusions and Recommendations

The scope of this thesis, as presented in the introduction, concerns one main objective. *“How to instrument an offshore nautical radar mounted on a mast structure for monitoring vibrations in operating conditions?”*. In order to reach the goal of recommending a sensor network set-up for the long term monitoring of the radar antenna, two series of modal analysis took place. Firstly, an [EMA](#) on the radar antenna itself and secondly an [OMA](#) on the mast that supported it. By examining the two structures and identifying some of their modal properties, certain conclusions were drawn regarding the formulated sub-questions given in [Chapter 1](#). In addition, it was shown how the acquired results can facilitate any future radar monitoring campaign, by taking into account environmental and operational limitations and by suggesting certain monitoring techniques. The aforementioned conclusions, along with recommendations for future studies and improvements are presented in the below sections.

7.1. Conclusions

The answers to the main research questions of [Chapter 1](#) can now be formulated as follows:

- How to collect and process the preliminary data for a non-rotating radar and a mast?

The first challenge faced on this research was how to instrument the non-rotating radar antenna with the limited available equipment, as presented on [Chapter 4](#), in order to extract the necessary modal properties. By taking into account the structure’s size and shape, [EMA](#) was deemed the fittest approach. As an input-output [SI](#) method, it can provide more deterministic outcomes, given that the top of the mast could approximate a laboratory environment when wind is minimal/non-present. A large number of grid points was selected in order to ensure that expected modes of vibration can be sufficiently captured in the z-direction. The first 4 modes of the radar antenna were successfully identified. The separate modal analysis of the plate that supports the antenna lead to the determination of another 2 (local) modes, which one of them proved to be part of one of the global modes of the radar antenna, which is justified by the fact that the system is coupled ([Table 7.1](#)). The structure showed as well linear response, which can be assumed to stay linear for non-extreme loading conditions.

7. Conclusions and Recommendations

Table 7.1.: Summary of the radar antenna's natural frequencies as presented in Chapter 4

Mode	Natural Frequency (Hz)
1	4,5
2	23
3	44
4 (plate)	74
5 (plate)	174

On the other hand, the mast vibration measurements proved a much more demanding task, as available equipment was not sufficient to extract concrete results about its structural behaviour. The instrumented hammer was not sufficient to provide enough energy to induce vibrations all across the mast's height, while the number of sensors and their cable length did not allow well distributed measurements points. Nevertheless, since OMA is a fitting SI method for large civil structures, an attempt was made to extract the natural frequencies of the first bending modes, by placing sensors on the top of mast in the two principal directions and using the ambient wind load as the source of excitation. By employing the NExT/ERA combination, several frequencies were identified (Table 7.2). The first two identified modes were in line both in direction and frequency with the FEM determined ones from Sfetsios [2022], especially when taking into account the FEM uncertainties. Although the number of sensors did not allow the capture of a mode shape, the similarities of the results with FEM model allow to come to the conclusion that they correspond to the mast's first two bending modes. An additional number of modes was identified through ERA, leading to further deductions that are examined on the next sub-question.

Table 7.2.: Summary of mast modes for both examined directions as presented in Chapter 5

Mode	Natural Frequency (Hz)
1 (x)	2
2 (y)	3
3 (y)	22
4 (y)	40
5 (x)	63
6 (y)	79
7 (y)	120
8 (y)	160
9 (x)	183

- How to distinguish the radar's dynamic response from the mast response?

Since the distinction of the responses of the two structures proved a difficult task to be realised during the time limitations of this thesis, an attempt was made instead to see how the results of the two modal analyses can be utilized to investigate how the mast's response may affect the radar's. This constituted the main reasoning behind the placement of the sensors on the top of the mast. By placing the sensors at this location, mast response data can be directly linked to the base motion of the radar

system. The first derivation from the vibration results of the two structures is the potential existence of two closely spaced modes (23 and 22 Hz). Since it is a coupled system, excitation frequencies close to these modes, could amplify the response of the antenna significantly, further contributing to the antenna's instability and in return to the fatigue accumulation. Another advantage from having identified natural frequencies from both structures is that any future researcher that will perform long term vibration measurements on the radar, under operational conditions, will be able to distinguish if any present frequency peaks may come from the vibration of the mast or from environmental loading.

- What kind of measurement equipment is suitable (e.g. accelerometer, DAQ) for monitoring vibrations on a rotating nautical radar?

By taking into account all the outcomes from *EMA*, a number of parameters were determined considering the instrumentation of a rotating nautical radar antenna, as summarized on [Table 7.3](#) and analyzed as follows:

- The suitable accelerometer specifications were determined. The frequency range was determined at 1-10000 Hz and acceleration amplitude at 50-100g.
- The sampling rate of 20000 Hz was found enough to capture all the well excited frequencies
- The appropriate measurement points and locations were able to be suggested by taking into account the potential nodal points and the parts of the radar that the vibration energy can be transmitted (energy could be transmitted only on the y-direction).
- the linearity of the structure's response was demonstrated.
- the natural frequencies of the radar antenna were identified ([Table 7.1](#)) along with corresponding mode shapes and quality factors. This can allow any future researcher to associate any other peaks in the spectral density with external loading or structure interaction.
- various wireless sensor network parameters were set.

Table 7.3.: Identified parameters checklist

Parameters	Identification
Acceleration amplitude	✓
Frequency range	✓
Sampling rate	✓
Measurements points	✓
Measurement locations	✓
Response linearity	✓
Modal properties	✓
Sensor network type	✓

7.2. Recommendations

- A series of uncertainties on the results comes from the fact that between the antenna and the top of the mast, the pedestal and the gearbox are intertwined. These structural components contribute to the the radar's response with their own respective vibrations. A modal analysis of these components can give a more comprehensive overview on how any "external" loading may affect the radar's response.
- Current research took place by only employing a minimal number of wired sensors. This fact put a lot of constraints regarding how deterministic the results could be, specifically in the case of the mast. By using a large number of sensors, distributed along the whole height and width of the structure, along with a wireless sensor network, the modal properties of the mast can be determined by using the same *OMA* techniques and algorithms used in this study. By knowing more about the structural behaviour of the mast, the interaction and the effect that it may have on the radar's structural integrity may be clearly established. As shown in [Sfetsios \[2022\]](#), the vibrations induced to the radar from the mast, appear to be the governing loading condition and main source of fatigue.
- Various vibration-based damage detection method are presented on [Chapter 6](#). A further study on these methods is deemed necessary in order to estimate the fatigue of the structure experimentally. In fact, the radar antenna poses a complex structure, for which material properties are also unknown, and these methods may not prove enough on their own. Considering this, the expected types of damages may only be roughly assumed. This is why a set of strain gauges in a large number of locations can prove an effective way to detect local damages and facilitate the fatigue analysis of the radar antenna.
- By employing the antenna's identified modal properties, the *FEM* model developed by [Sfetsios \[2022\]](#) can be updated now with real data, and thus create a more representative model that can be further used to further support the structural health monitoring process.

A. EMA daily log

Metal plate test

Day 1 Log: 20/12/2021 (3 oC, 1 Beaufort, dry)

I distributed 10 impact points (including the one with the accelerometer), 10cm apart starting from both edges. Far right point is No. 11 and far left is No. 20. Close to center is not possible to measure due to the presence of the gearbox.

I attached (glued) PCB352a24 (uniaxial, 50g pk) to the far right measurement point (Point 11), since we are interested in the z principal direction for the plate and we expect the biggest amplitudes close to the edges. I secured the cable on the pedestal with tape. I set the sensitivity in SignalExpress accordingly to the calibration certificate of the accelerometer and the sampling rate for the DAQ at 5000 Hz. All adjustments were done on the Test1 file used for the TU Delft labs.

Check for appropriate hammer tip. I began with the medium impact cap, but I could not avoid double tapping. I continued with the hard impact cap (steel) and again was really difficult to avoid double tap. I added the extra weight and then I achieved "clean" impacts all across the metal plate.

I did a preliminary process of the recording with hammer analysis.mat and I noticed accelerations below 50g and frequencies well excited below the 2000 Hz point. That's why I set a sample rate of 20000 Hz.

I began measurements by impacting really close to the output point (Point 11). Most of the times I got weird acceleration time series. (Due to present accelerations above 50g which is the peak of the accelerometer).

I managed to get "normal" readings though, when acceleration levels were below 50g. I did not change the accelerometer, since in every other impact point, acceleration levels weren't above 30g.

I performed 5 impacts per point, since the wind was weak. I managed to measure only 5 of the 10 points (11-15). It was too cold to continue and clean hammer impacts were becoming hard to perform. I also left the reciprocity test for the next time for the same reason.

Day 2 Log: 22/12/2021 (1 oC, 2 Beaufort, dry)

A. EMA daily log

I attached (glued) PCB352a24 (uniaxial, 50g pk) to the measurement point (Point 2'), Since we are interested in the z principal direction for the radar antenna and we expect the biggest amplitudes close to the edges. I secured the cable on the pedestal with tape. I set the sensitivity in SignalExpress accordingly to the calibration certificate of the accelerometer and the sampling rate for the DAQ at 20000 Hz. (steel impact tip, extra weight). I performed measurements for reciprocity, by impacting measurement point 11 and measuring accelerations in point 12. I also recorded an ambient measurement. I switched accelerometer back to measurement point 11. I performed impact tests for points 6 through 10 (5 impacts per point).

Day 3 Log: 23/12/2021 (3 oC, 3-4 Beaufort, dry)

No measurements were performed due to strong wind and cold weather.

Radar antenna test

Day 4 Log: 24/01/2022 (5 oC, 2 Beaufort, dry)

I attached (glued) PCB352a24 (uniaxial, 50g pk) to the measurement point (Point 2), since we are interested in the z principal direction for the plate and we expect the biggest amplitudes close to the edges. I secured the cable on the pedestal with tape. I set the sensitivity in SignalExpress accordingly to the calibration certificate of the accelerometer and the sampling rate for the DAQ at 20000 Hz. (steel impact tip, extra weight). I used the metal hammer tip along with the extra weight as with the plate measurements. I noticed accelerations below 50g so I kept the already chosen accelerometer. I set a sample rate of 20000 Hz as with the plate. I performed measurements for points 1, 2-10 (composite antenna part) and 11-13 (metal plate). 5 hammer impacts per point.

Day 5 Log: 26/01/2022 (5 oC, 3 Beaufort, dry)

I attached (glued) PCB352a24 (uniaxial, 50g pk) to the measurement point (Point 9) to perform reciprocity measurements. I attached (glued) PCB352a24 (uniaxial, 50g pk) to the measurement point (Point 2), since we are interested in the z principal direction for the plate and we expect the biggest amplitudes close to the edges. I secured the cable on the pedestal with tape. I set the sensitivity in SignalExpress accordingly to the calibration certificate of the accelerometer and the sampling rate for the DAQ at 20000 Hz. (steel impact tip, extra weight). I used the metal hammer tip along with the extra weight. I performed measurements for points 14-18 (metal plate). 5 hammer impacts per point. Hardware or software malfunction – measurements terminated

Day 6 log: 04/03/2022 (10 oC, 3 Beaufort, dry)

Change of output point to 28 due to inconclusive/broken data from previous days same parameters. Measurements in points 16-26

Day 7 log: 09/03/2022 (11 oC, 2-3 Beaufort, dry)

Point 28 as output. Measurements in points 27-30, 1-15
Points 27-30, with extra weight off (28)

Day 8 log: 11/03/2022 (14 oC, 4 Beaufort, dry)

Re-measurement of minor number of points with broken data

Bibliography

- Avci, O. (2020). A review of vibration-based damage detection in civil structures: From traditional methods to machine learning and deep learning applications. *Mechanical Systems and Signal Processing*.
- Bocca, M. (2011). A synchronized wireless sensor network for experimental modal analysis in structural health monitoring. *Computer-Aided Civil and Infrastructure Engineering*.
- Brandt, A. (2011). *Noise and Vibration Analysis: Signal Analysis and Experimental Procedures*. Wiley.
- Cabboi, A. (2016). Automated modal identification and tracking: Application to an iron arch bridge. *STRUCTURAL CONTROL AND HEALTH MONITORING*.
- Caicedo, J. (2011). Practical guidelines for the natural excitation technique (next) and the eigensystem realization algorithm (era) for modal identification using ambient vibration. *Dynamic Testing of Civil Engineering Structures Series*.
- Carden, E. (2008). Arma modelled time-series classification for structural health monitoring of civil infrastructure. *Mechanical Systems and Signal Processing*.
- Chauchan, S. (2011). Operational modal analysis of operating wind turbines: Application to measured data. *XXIX International Modal Analysis Conference*.
- Cicirello, A. (2020). Data, vibration and uncertainty group (dву).
- Cuhna, A. (2006). Experimental modal analysis of civil engineering structures. *SOUND AND VIBRATION*.
- Damgaard, M. (2011). An introduction to operational modal identification of offshore wind turbine structures. *Department of Civil Engineering, Aalborg University. DCE Technical Memorandum No. 13*.
- Das, S. (2015). Vibration-based damage detection techniques used for health monitoring of structures: a review. *J Civil Struct Health Monit (2016) 6:477–507*.
- Derrick, T. (2004). Time series analysis: The cross-correlation function.
- Gasparis, G. (2019). A benchmark study on operational modal analysis system identification algorithms for operating offshore wind turbines.
- Gentile, C. (2015). Structural identification of a masonry tower based on operational modal analysis. *International Journal of Architectural Heritage*.
- Grimmelsman, K. (2014). Operational modal analysis of a truss bridge under different excitation cases. *Bridge Maintenance, Safety, Management and Life Extension*.

Bibliography

- Guan, H. (2006). Web-based structural health monitoring of a frp composite bridge. *Computer-Aided Civil and Infrastructure Engineering*, 21, 39–56.
- Gul, M. (2008). Ambient vibration data analysis for structural identification and global condition assessment. *JOURNAL OF ENGINEERING MECHANICS* © ASCE.
- Gul, M. (2009). Statistical pattern recognition for structural health monitoring using time series modeling: Theory and experimental verifications. *Mechanical Systems and Signal Processing*.
- Karbhari, V. (2009). Operational modal analysis for vibration-based structural health monitoring of civil structures. *Structural health monitoring of civil infrastructure systems*, 213-259.
- Kopsaftopoulos, F. (2010). Statistical pattern recognition for structural health monitoring using time series modeling: Theory and experimental verifications. *Mechanical Systems and Signal Processing*.
- Lestari, S. (2007). Curvature mode shape-based damage assessment of carbon/epoxy composite beams. *Journal of Intelligent Material Systems and Structures*.
- Magalhaes, F. (2011). Vibration based structural health monitoring of an arch bridge: From automated oma to damage detection. *Mechanical Systems and Signal Processing*.
- Miguel, L. (2012). Damage detection under ambient vibration by harmony search algorithm. *Expert Systems with Applications*.
- Nayeri, R. (2009). Study of time-domain techniques for modal parameter identification of a long suspension bridge with dense sensor arrays. *JOURNAL OF ENGINEERING MECHANICS*.
- Pappalardo, C. (2018). System identification and experimental modal analysis of a frame structure. *Engineering Letters*.
- Sfetsios, V. (2022). Development of a dynamic model of a nautical radar on a mast structure for fatigue damage analysis. *TU Delft Thesis*.
- Sohn, M. (2007). Effects of environmental and operational variability on structural health monitoring. *Vol. 365, No. 1851, Structural Health Monitoring*.
- Tirelli, D. (2011). Modal analysis of small medium structures by fast impact hammer testing method. *European Commission - Joint Research Centre*.
- Venglar, M. (2019). Experimental modal analysis of diagonal members. *Vibroengineering PROCEDIA*.
- Whelan, M. (2009). Real-time wireless vibration monitoring for operational modal analysis of an integral abutment highway bridge. *Engineering Structures*, 30(10), 2224–35.
- Whelan, M. (2010a). Operational modal analysis of a multi-span skew bridge using real-time wireless sensor networks. *Journal of Vibration and Control*.
- Whelan, M. (2010b). Wireless operational modal analysis of a multi-span prestressed concrete bridge for structural identification. *Smart Material and Structures*, 6(5-6), 579–93.
- Wu, J. (2022). Experimental modal analysis of a rotating tendon-loaded helicopter blade demonstrator. *Mechanical Systems and Signal Processing*.
- Yin, T. (2009). Dynamic reduction-based structural damage detection of transmission tower utilizing ambient vibration data. *Engineering Structures*.

Colophon

This document was typeset using \LaTeX , using the KOMA-Script class `scrbook`. The main font is Palatino.

